

A century of reduced ENSO variability during the Medieval Climate Anomaly

A.E. Lawman^{1,2*}, T.M. Quinn^{1,2}, J.W. Partin¹, K. Thirumalai^{1,3}, F.W. Taylor¹, C.-C. Wu^{4,5}, T.-L Yu^{4,5}, M.K. Gorman^{1,2}, C.-C. Shen^{4,5}

¹Institute for Geophysics, Jackson School of Geosciences, The University of Texas at Austin, Austin, TX, USA, ²Department of Geological Sciences, Jackson School of Geosciences, The University of Texas at Austin, Austin, TX, USA, ³Department of Earth, Environmental and Planetary Sciences, Brown University – Providence, RI, USA, ⁴High-precision Mass Spectrometry and Environment Change Laboratory (HISPEC), National Taiwan University, Taipei, Taiwan ROC, ⁵Research Center for Future Earth, National Taiwan University, Taipei, Taiwan ROC

*Corresponding author: Allison Lawman (alawman@utexas.edu)

This is a non peer-reviewed preprint submitted to EarthArXiv. The article was submitted to *Paleoceanography and Paleoclimatology* on July 31, 2019.

Key Points:

- Vanuatu coral Sr/Ca-SST variations are a proxy of El Niño-Southern Oscillation (ENSO) variability
- Vanuatu fossil coral Sr/Ca-SST variations indicate one hundred years of lower ENSO variability during part of the Medieval Climate Anomaly
- Periods of reduced ENSO variability can last a century, far longer than modern observations in the instrumental record of ENSO

1 **Abstract**

2 Climate model simulations of El Niño-Southern Oscillation (ENSO) behavior for the last
3 millennium demonstrate interdecadal to centennial changes in ENSO variability that can arise
4 purely from stochastic processes internal to the climate system. However, the instrumental record
5 of ENSO does not have the temporal coverage needed to capture the full range of natural ENSO
6 variability observed in long, unforced climate model simulations. Here we demonstrate a
7 probabilistic framework to quantify changes in ENSO variability via histograms and probability
8 density functions using monthly instrumental and coral-based sea surface temperature (SST)
9 anomalies from 1900-2005 CE and 1051-1150 CE. We find that reconstructed SST anomalies from
10 modern corals from the southwest Pacific capture changes in ENSO variability consistent with
11 instrumental SST data from the central equatorial Pacific. Fossil coral records indicate one hundred
12 years of relatively lower ENSO variability during part of the Medieval Climate Anomaly. Our
13 results demonstrate that periods of reduced ENSO variability can last a century, far longer than
14 modern observations in the instrumental record of ENSO, but consistent with results from unforced
15 climate model simulations.

16 **Plain Language Summary**

17 The chemistry of coral skeletal material is a passive recorder of environmental conditions, like the
18 temperature of the water in which the coral lives. For example, the ratio of the element strontium
19 (Sr) to the element calcium (Ca) in the coral skeleton will vary in response to changes in sea surface
20 temperature (SST). Paleoclimatologists measure coral Sr/Ca to determine how SSTs vary in the
21 past. In this study, we use corals from the southwest Pacific to understand how SSTs in the tropical
22 Pacific Ocean varied during the 20th century and ~900 years ago during a time interval called the
23 Medieval Climate Anomaly. We focus on SST variability related to the El Niño-Southern
24 Oscillation (ENSO), a climate phenomenon that operates on year-to-year timescales and impacts
25 global temperature and rainfall patterns. Here we use temperatures estimates inferred from corals
26 and find that past changes in ENSO variability during part of the Medieval Climate Anomaly is
27 similar to the early part of the 20th century.

28 **1 Introduction**

29 The El Niño-Southern Oscillation (ENSO) is a coupled ocean-atmosphere climate phenomenon
30 with global impacts on temperature and precipitation patterns [*Bjerknes, 1969; Ropelewski and*
31 *Halpert, 1987*]. ENSO is the leading mode of interannual (>1-9 year) climate variability, but
32 instrumental observations are of insufficient length [*Deser et al., 2010*] to characterize the full
33 range of natural variability [*Wittenberg, 2009*]. Given the wide range of ENSO behavior simulated
34 in the absence of forcings external to the climate system [*Wittenberg, 2009; Deser et al., 2012*], it
35 is critical to ascribe the degree to which anthropogenic warming and internal climate variability
36 are each contributing to future projections of ENSO in climate models [*Collins et al., 2010;*
37 *DiNezio et al., 2013*]. This motivates the use of paleo-ENSO reconstructions as out-of-sample tests
38 of climate model simulations [*Gagan et al., 2000; Cobb et al., 2013*].

39
40 Isolating the unforced and forced components of ENSO variability remains an ongoing challenge
41 in paleoclimate science, particularly for different mean climate states when forcings were different
42 from today (e.g., the mid-Holocene or the Last Glacial Maximum) [*Masson-Delmotte et al., 2013;*
43 *Liu et al., 2014*]. Focusing on ENSO variability over the last two thousand years (the Common

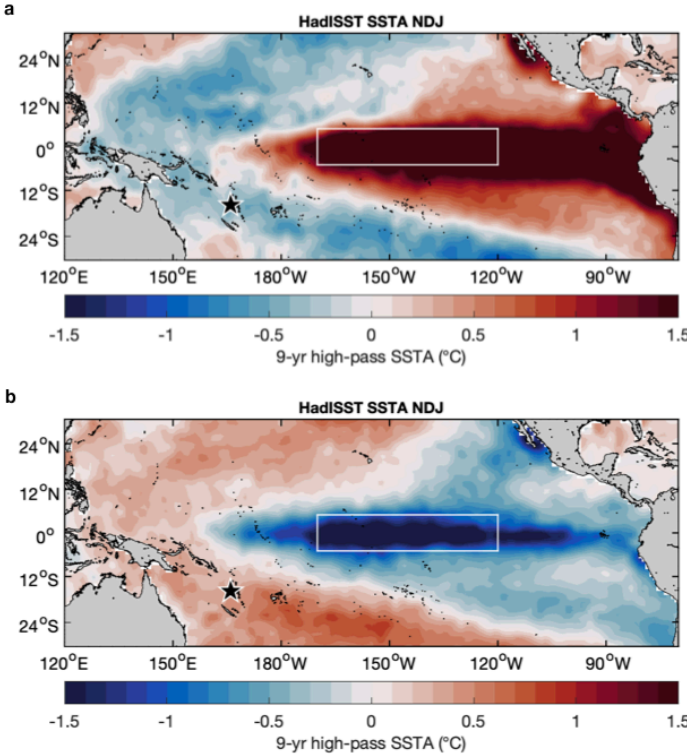
44 Era, CE), provides context for the understanding of natural ENSO variability with current and
45 near-future climate change. The Medieval Climate Anomaly (MCA: 950-1250 CE [*Masson-*
46 *Delmotte et al.*, 2013]) is identified as an interval with Northern Hemisphere surface temperatures
47 similar to the modern [*Masson-Delmotte et al.*, 2013], but our understanding of paleo-ENSO
48 variability is inadequate due to a limited number of sub-annually resolved proxy records over the
49 last millennium [*Emile-Geay et al.*, 2013a; 2013b]. Furthermore, given that the magnitude of
50 orbital [*Bertrand et al.*, 2002], solar [*Bard et al.*, 2000], and volcanic [*Crowley*, 2000; *Gao et al.*,
51 2008] forcing during the MCA is both small and similar to the modern (pre-industrial), sustained
52 changes in ENSO variability are likely dominated by processes internal to the climate system
53 [*McGregor et al.*, 2013; *Rustic et al.*, 2015].

54
55 Coral records of surface ocean conditions extend our knowledge of interannual tropical climate
56 variability to places and times when there is no (or limited) instrumental data [*Fairbanks et al.*,
57 1997; *Gagan et al.*, 2000; *Corrège*, 2006]. Traditionally, coral-based ENSO reconstructions use
58 the standard deviation of a band-pass filtered time series (2-7 year window) of coral geochemical
59 proxies as a metric of past ENSO variability [*Cobb et al.*, 2003; 2013; *Hereid et al.*, 2013b; *Emile-*
60 *Geay et al.*, 2016], but this approach 1) filters out, by mathematical construction, important ENSO
61 variance that has a period of less than two years, and 2) necessitates many decades and longer
62 continuous datasets. Many fossil coral records, particularly older Holocene or Last Glacial
63 Maximum corals, are short (several decades or less) or discontinuous, and thus ill-suited for
64 traditional filtering and data analysis methods [*Tudhope*, 2001; *Cobb et al.*, 2013]. To address
65 these challenges, we extend the procedure suggested in *Trenberth* [1997] and use descriptive
66 statistics in tandem with probability theory by assessing histograms [*Trenberth*, 1997] and
67 probability density functions (PDFs) [*Parzen*, 1962] of monthly resolved coral data to quantify
68 changes in ENSO variability.

69
70 The Niño 3.4 SST index is a well-recognized record of ENSO variability [*Trenberth et al.*, 2002];
71 however, conditions in other regions of the tropical Pacific, notably the southwest Pacific, also
72 accurately record changes in ENSO variability [*Hereid et al.*, 2013a]. Departures from the long-
73 term monthly mean SST, (SST anomalies; SSTA) from the Niño 3.4 region (5°N-5°S, 120°-
74 170°W, Figure 1, box) in the central equatorial Pacific are canonically used to define the
75 occurrence of ENSO events [*Trenberth*, 1997]. To isolate interannual variability, we compute
76 monthly SST anomalies by applying a 9-year high-pass filter to the SST data (to remove decadal
77 and longer variance), removing the monthly mean climatology for the 1961-1990 CE reference
78 period (to remove annual cycle variance), and computing the 5-month-running mean (to smooth
79 out variance related to intraseasonal variations) [*Trenberth*, 1997] (Section 3.3). During El Niño
80 (La Niña) events, the central and eastern tropical Pacific experience positive (negative) SST
81 anomalies that peak during boreal winter, while the western tropical Pacific experiences negative
82 (positive) excursions [*Trenberth*, 1997] (Figure 1). Many paleo-ENSO studies target the Niño 3.4
83 region [*Cobb et al.*, 2003; *Nurhati et al.*, 2009], but other regions of the Pacific, like the tropical
84 southwest Pacific in the South Pacific Convergence Zone, are also sensitive to ENSO variability,
85 with ENSO detection skill broadly similar to the Niño 3.4 region (60-70% skill) [*Hereid et al.*,
86 2013a]. The tropical southwest Pacific is also advantageously home to abundant, high-quality
87 modern and fossil corals, making this region a suitable location for paleo-ENSO studies [*Quinn et*
88 *al.*, 1996; *Linsley et al.*, 2006; *Quinn et al.*, 2006; *Gorman et al.*, 2012; *Hereid et al.*, 2013b]. We
89 also concentrate our efforts on reconstructing decadal to interdecadal changes in paleo-ENSO

90 variability, rather than reconstructing the month-to-month changes of SST in the Niño 3.4 region,
91 as this is difficult to reconstruct back in time due to age uncertainties [Emile-Geay et al., 2013a;
92 2013b].
93

94 Here we use modern corals from Vanuatu, an archipelago in the southwest Pacific (Figure 1, star),
95 to document ENSO variability during the 20th century, and fossil corals to determine ENSO
96 variability during the MCA. This tropical location experiences a consistent SST response during
97 ENSO events, as evidenced in the recent decades of instrumental data: cooler SSTs during El Niño
98 events (Figure 1a) and warmer SSTs during La Niña events (Figure 1b). Fieldwork at Vanuatu
99 identified and recovered abundant, high-quality modern and fossil *Porites lutea* corals well-suited
100 for ENSO variability studies (Section 2.1). Due to the tectonic activity of south Pacific islands like
101 Vanuatu [Taylor et al., 1987], the rate of uplift outpaces sea-level rise, which exposes fossil corals
102 above present day sea level. Another unique feature of our study site is that the fossil coral heads
103 are all *in situ* [Thirumalai et al., 2015], allowing us to better understand the morphology of the
104 reef flat, and use estimates of the uplift rate to constrain the water depth in which the corals lived.
105 We first demonstrate our data analysis technique by quantifying instrumental SST variability in
106 the Niño 3.4 region and then apply our methods to replicated coral Sr/Ca-SST records from the
107 southwest Pacific.



108
109 **Figure 1. Instrumental sea surface temperature anomalies during strong ENSO events.** a Average November-
110 December-January (NDJ) sea surface temperature anomalies (SSTA) for the 1972-73, 1982-83, and 1997-98 El Niño
111 events. b Average NDJ SSTA for the 1988-89, 1995-96, 1998-99 La Niña events. SST data from the Met Office
112 Hadley Centre HadISST product [Rayner et al., 2003]. SSTA in this study are computed by applying a 9-year high-
113 pass filter to monthly SST data, removing the climatology, and calculating the 5-month running mean [Trenberth,
114 1997] SSTA (Section 3.3). The Niño 3.4 region (5° N-5°S, 120°-170°W) in the central equatorial Pacific is outlined
115 by a white box (a, b). The modern coral site at Sabine Bank, Vanuatu in the southwest Pacific (15.9°S, 166.0°E) is
116 indicated with a star (a, b).

117 2 Materials and Methods

118 2.1 Coral Selection and Sampling

119
120 We located pristine, well-preserved, *in situ* fossil *P. lutea* coral heads spanning the last two
121 millennia from an uplifted reef offshore of Tasmaloum, Vanuatu (TMV: 15.6 °S, 166.9 °E). The
122 cores were drilled using a Stihl chainsaw equipped with a Pomeroy Gear-Reduced Core Drill and
123 diamond coring bits. All coral cores were uranium-thorium (U-Th) dated at the High-precision
124 Mass Spectrometry and Environment Change Laboratory (HISPEC), National Taiwan University,
125 using multi-collector inductively coupled plasma mass spectrometry (MC-ICP-MS) [Shen *et al.*,
126 2012; Cheng *et al.*, 2013]. Table S1 provides a summary of the properties for the selected modern
127 and fossil corals. This study uses fossil corals 11-TM-S5 ($^{230}\text{Th} \pm 2\sigma$ age: 1127.1 ± 2.7 CE, 36.4
128 cm depth) and 11-TM-I1 ($^{230}\text{Th} \pm 2\sigma$ ages: 1125.7 ± 6.2 CE, 30.5 cm depth; 1142.6 ± 4.9 CE, 18.0
129 cm depth; 1149.0 ± 4.1 CE, 10.7 cm depth). Based on estimates of the uplift rate (~ 5.5 mm/yr)
130 [Taylor *et al.*, 1990], the selected fossil coral heads grew approximately 1-3 m below the sea
131 surface during the Medieval Climate Anomaly.

132
133 To provide modern climatological context, the analysis incorporated core 06-SB-A1 collected
134 from a live *P. lutea* coral head at 8 m water depth at Sabine Bank, Vanuatu (SBV: 15.9 °S, 166.0
135 °E), ~ 90 km to the southwest of TMV. Core 06-SB-A1 was collected using the French Research
136 Institute for Development (IRD) vessel R/V *Alis*. To quantify the replication uncertainty in our
137 modern coral reconstructions, we also incorporated 50 years (1941-1990 CE) of published modern
138 coral Sr/Ca data from Malo Channel, Vanuatu (MCV: 15.7 °S, 167.2 °E) [Kilbourne *et al.*, 2004].

139
140 X-ray images of 5 mm slabs extracted from the coral cores (Figure S1) highlighted the annual
141 density banding and the optimal sampling paths along the maximum growth axis. All slabs were
142 sonicated in distilled water and air dried prior to sampling. The coral slabs were micro-milled at
143 approximately monthly resolution (12 points/yr) following established protocols [DeLong *et al.*,
144 2013]. The sampling resolution varied from 0.5-1.0 mm depending on the average growth rate of
145 each respective coral (Table S1). The coral slabs were x-ray imaged a second time after micro-
146 milling (Figure S1) to confirm that the sampling paths were parallel to the growth direction of
147 individual corallites and along the central axis of a radially extending corallite fan [DeLong *et al.*,
148 2013].

149
150 To develop a reliable Sr/Ca-SST record, it is critical to ensure that the coral is sampled along the
151 maximum growth axis. We therefore considered how the coral growth architecture in three
152 dimensions is projected in the 2-D plane of the cross-sectional slabs. In the case of fossil coral 11-
153 TM-S5, we extracted additional 5 mm slabs from the core (Figure S1) to generate a continuous
154 record and ensure that the resultant Sr/Ca composite passed all of the quality control metrics
155 outlined in DeLong *et al.* [2013]. Sections with visible stress banding in the x-ray images and a
156 lack of clearly defined theca walls (e.g. the bottom of the 11-TM-I1 replication fossil coral; Figures
157 S1 and S3) are also sub-optimal as this can impact the annual cycle in the geochemistry [Marshall
158 and McCulloch, 2002] and/or make it difficult to identify the maximum growth axis for sampling.
159 Sub-optimal sampling can lead to unreliable climate reconstructions, so we excluded sampling
160 paths that did not pass the quality control metrics of DeLong *et al.* [2013], and conservatively limit
161 our climate interpretations to the final Sr/Ca composites presented herein.

162

163 2.2 Coral Sr/Ca Analyses

164
165 Elemental ratio analyses were conducted using a Perkin Elmer Optima 8300 inductively coupled
166 plasma – optical emission spectrometer (ICP-OES) located at UT Austin. All Sr/Ca measurements
167 were corrected for plasma drift using standard-sample bracketing techniques [Schrag, 1999] with
168 an internal reference solution gravimetrically prepared to have Ca, Sr, and Mg proportions similar
169 to that of a coral. For each analysis, 113-262 μg of carbonate powder was dissolved in 2 wt. %
170 nitric acid such that the Ca^{2+} concentration in each sample was approximately 20 ppm, and within
171 our 8-32 ppm calibration range for Ca^{2+} .

172
173 The long-term precision of the Sr/Ca measurements for the 11-TM-S5, 11-TM-I1, and 06-SB-A1
174 samples is $\pm 0.05\%$ (2σ ; 0.009 mmol/mol) based on repeated measurement ($n > 7,500$) of an
175 internal gravimetric standard, and $\pm 0.06\%$ (2σ ; 0.012 mmol/mol) based on repeated measurement
176 ($n > 800$) of a homogenized coral powder from a *P. lutea* coral collected from Efate, Vanuatu
177 (17.7°S , 168.3°E) dissolved in 2 wt. % nitric acid. The analytical precision for the published MCV
178 Sr/Ca data is 0.15% ($\pm 2\sigma$; 0.013 mmol/mol) based on 86 measurements of an in-house coral
179 standard [Kilbourne *et al.*, 2004].

180 181 2.3 Coral Sr/Ca Composites and Age Modeled Timeseries

182
183 X-ray images of the micro-milled coral slabs (Figure S1) provided clear constraints on the amount
184 of overlap between two sampling paths, and the strong seasonal cycle observed in coral Sr/Ca was
185 used to align peaks and troughs over the common period of overlap and generate the final Sr/Ca
186 composite records. For a given year in the coral time series, the highest Sr/Ca value indicates the
187 climatological coldest month, whereas the lowest Sr/Ca value indicates the climatological warmest
188 month. To convert Sr/Ca vs. depth to Sr/Ca vs. time, we used a MATLAB® algorithm to identify
189 the Sr/Ca peaks and troughs and linearly interpolate the data to 12 points/yr.

190
191 The relative age model for the modern SBV coral was converted to calendar years by counting
192 back from the date of collection, whereas the relative chronologies for the fossil corals were
193 converted to calendar years using four ^{230}Th ages as tie points (Table S1). The fossil coral Sr/Ca
194 time series were shifted within the analytical error ($\pm 2\sigma$) of the four ^{230}Th ages (Figure S3) such
195 that the resulting overlap between 11-TM-S5 and 11-TM-I1 achieved the highest Pearson
196 correlation coefficient [Pearson, 1920] ($r = 0.81$, $p < 0.01$). We interpolated the published MCV
197 modern coral Sr/Ca [Kilbourne *et al.*, 2004] vs. time data to 12 points/yr using a piecewise cubic
198 hermite interpolating polynomial [Fritsch *et al.*, 1980].

199

200 3 Data Processing and Uncertainty Analysis

201 3.1 Instrumental Sea Surface Temperature (SST) Data

202
203 All instrumental SST data is from the Met Office Hadley Centre 1° latitude x 1° longitude gridded
204 product (HadISST) [Rayner *et al.*, 2003]. SST data for the Niño 3.4 region was averaged over the
205 (5°S - 5°N , 120° - 170°W) domain (Figure 1 box). The 20th century historical ENSO events are based
206 on the Oceanic Niño Index (NOAA:
207 http://origin.cpc.ncep.noaa.gov/products/analysis_monitoring/ensostuff/ONI_v5.php) and the

208 multi-variate ENSO index [Wolter and Timlin, 2011]. For Vanuatu, we averaged the SST data
209 from the two nearest grid points to the coral sites (15.5°S, 166.5°E) and (16.5°S, 166.5°E). We
210 averaged the two SST series such that the resulting SST series better represented the range of SST
211 observed in 7.75 years (Nov. 1999 - July 2007) of *in situ* SST logger data from Sabine Bank,
212 Vanuatu [Ballu *et al.*, 2013].

213

214 3.2 Proxy Calibration (Sr/Ca-SST)

215

216 We used the modern SBV coral Sr/Ca composite and gridded SST for Vanuatu to perform a
217 calibration-verification exercise [Quinn and Sampson, 2002] (Figure S2). We applied the
218 following linear calibration to all age-modeled modern and fossil coral Sr/Ca measurements: SST
219 (°C) = -20.73 x Coral Sr/Ca (mmol/mol) + 210.53. To determine this calibration equation, we
220 performed a weighted bivariate regression [Thirumalai *et al.*, 2011] of the SST annual cycle
221 (defined as the maximum SST – minimum SST) vs. the SBV coral Sr/Ca annual cycle over the
222 1985-2005 CE calibration window. When performing the weighted, bivariate regression, we
223 conservatively used 0.1 °C as the uncertainty in the instrumental SST, and the analytical
224 uncertainty (0.012 mmol/mol, $\pm 2\sigma$) as the uncertainty in coral Sr/Ca. The regression was force fit
225 through the origin to yield a slope value of -20.73 °C/mmol/mol. The y-intercept for the calibration
226 equation was empirically determined such that the median coral Sr/Ca-SST equaled the median
227 instrumental SST over the calibration interval.

228

229 We used 1985-2005 CE as the calibration interval because this window maximized the correlation
230 with instrumental SST ($r = 0.87$, $p < 0.01$) and also minimized the residual sum of squares over
231 the 1955 – 1984 CE verification window. We note that 4 other potential calibration intervals (1950-
232 2005 CE, 1971-2000 CE, 1980-2005, 1985-2004 CE) yielded similar slope values (range: -19.55
233 to -21.67 °C/mmol/mol) that were all within the range of published coral Sr/Ca-SST calibrations
234 [Corrège, 2006; DeLong *et al.*, 2010]. The coral trend of 0.83 °C/50 years at Sabine Bank
235 resembles the trend of 0.5-0.75°C/50 years seen in observations for the southwest Pacific [Cravatte
236 *et al.*, 2009].

237

238 3.3 SST Data Processing

239

240 We performed a series of mathematical operations to isolate variability at interannual (>1-9-yr)
241 timescales, the result of which preserves more variance than a 2-8-yr band-pass filter. Prior to
242 removing the climatology, we first applied a 9-year high-pass filter to the monthly instrumental
243 and monthly coral-based SST to remove decadal and longer variability. Monthly SST anomalies
244 were calculated as deviations from the 1961-1990 CE climatology for the tropical Pacific
245 composite map (Figure 1), the Niño 3.4 and Vanuatu instrumental SST, and the modern coral
246 Sr/Ca-SST. Monthly SSTA were calculated as deviations from the 1126-1145 CE climatology for
247 the MCA fossil corals. The climatology reference intervals were selected to maximize the temporal
248 overlap between contemporaneous records. Lastly, we computed a 5-month running mean of
249 monthly SSTA to smooth out intraseasonal variations [Trenberth, 1997]. All probability density
250 function estimates (PDFs) of the monthly SST and monthly SSTA data were computed using a
251 kernel density estimation method [Parzen, 1962]. All instrumental and coral-based monthly SST
252 anomaly results are reported as 9-year high-pass filtered, climatology removed, and 5-month
253 running mean SSTA.

254
255
256
257
258
259
260
261
262
263
264
265
266
267
268
269
270
271
272
273
274
275
276
277
278
279
280
281
282
283
284
285
286
287
288
289
290
291
292
293
294
295
296
297
298
299

3.4 Uncertainty Analysis

We quantify changes in variability using the extreme percentiles ($p_{2.5}$ and $p_{97.5}$) of monthly SST and SSTA distributions (Sections 5.1 and 5.2). We performed a Monte Carlo simulation ($n = 10,000$) to quantify the analytical and calibration uncertainties [Thirumalai *et al.*, 2014] in the 2.5 ($p_{2.5}$) and 97.5 ($p_{97.5}$) percentiles for the coral-based monthly SST and monthly SSTA distributions. We also used replicated coral Sr/Ca records to incorporate the effects of “geological” uncertainty, which is due to all other sources including the oceanographic setting, sampling, etc. We subset all contemporaneous coral Sr/Ca records to their common period of overlap when performing the Monte Carlo simulation (Modern corals: 1941-1990 CE; Fossil corals: 1126-1145 CE). We perturbed each data Sr/Ca data point in the original 50 (modern) or 20 (fossil) year-long time series n times with values randomly sampled from a normal distribution with mean zero and a standard deviation equal to the $\pm 2\sigma$ analytical uncertainty (± 0.012 mmol/mol). We then transformed each Sr/Ca realization into SST taking uncertainty in the proxy calibration into account. For each realization of the Sr/Ca time series, a slope value was randomly sampled from a normal distribution centered on the empirically determined slope for Vanuatu (-20.73 °C/mmol/mol) and a $\pm 2\sigma$ range that approximately spanned the range of published coral Sr/Ca-SST calibration slopes [Corrège, 2006; DeLong *et al.*, 2010]. A corrective factor was applied to the n realizations of the y-intercept such that the linear transformation for a given slope produced a y-intercept that yielded the mean SST for the unperturbed time series.

A 9-year high pass filter was applied to the n SST realizations prior to removing the climatology. The 5-month running mean SSTA was also computed as defined in section 3.3 above. For each realization of the SST and SSTA time series we computed the $p_{2.5}$ and $p_{97.5}$ values. The overall uncertainty is the $\pm 2\sigma$ range based on n realizations. In the event that the $p_{2.5}$ and $p_{97.5} \pm 2\sigma$ values slightly differed for a given coral, we averaged the two values as the combined effect of analytical and calibration uncertainty. The analytical and calibration uncertainty quantification for the modern SBV coral is provided as an example (Figure S4).

The total uncertainties including the effect of replication in the 2.5 and 97.5 percentiles of the SSTA distributions are reported as the root mean square error of the percentile uncertainties for each respective modern and fossil coral determined by the Monte Carlo simulation with analytical and calibration uncertainty discussed above.

To test whether coral Sr/Ca-SSTA come from the same distribution, we performed Kolmogorov-Smirnov (K-S) tests [Frank J Massey, 1951] at the 1% significance level. Given that the SSTA time series are serially correlated, the effective degrees of freedom were considered when assessing the significance [Hu *et al.*, 2017] of the K-S tests. Adjusting the effective degrees of freedom (v_{eff}) makes it more difficult to reject the null hypothesis that the two datasets are from the same distribution at a specified significance level. The statistical significance of the K-S tests is further described and discussed in the results section. We also further explored the fidelity of the differences in the $p_{2.5}$ and $p_{97.5}$ values taking the total uncertainty into account. We used the results from our uncertainty analysis (e.g. Figure S4) to examine the overlap between the $p_{2.5}$ and $p_{97.5}$ distributions (additional details provided in sections 5.1 and 5.2 and Figures S5-S7).

300 4. SST Variability in the Niño 3.4 Region

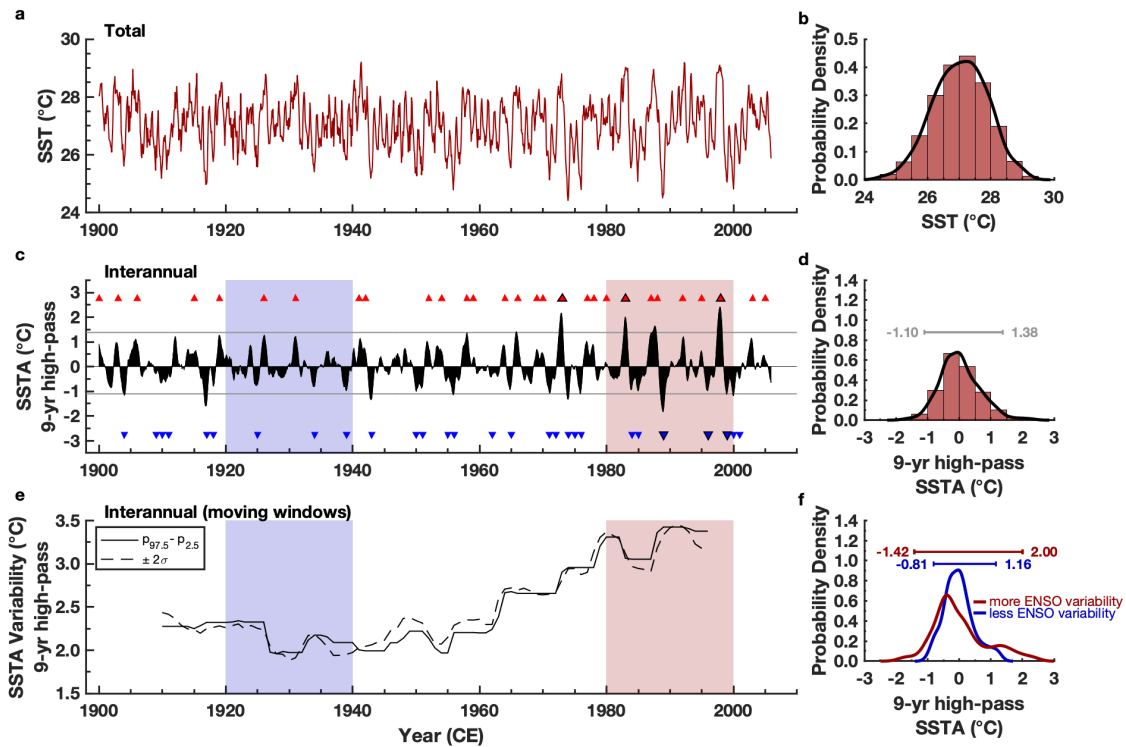
301
302 We use instrumental SST data from the Niño 3.4 region [Rayner *et al.*, 2003] (Figure 2a) as a test-
303 case to demonstrate how a probabilistic framework quantifies previously identified changes in 20th
304 century ENSO variability [Trenberth, 1976; Torrence and Compo, 1998]. We choose a time-
305 domain subset of 1900-2005 CE to temporally match the modern coral climate record from
306 Vanuatu. Prior research has often quantified ENSO variability using power spectra [Quinn *et al.*,
307 1996; Wittenberg, 2009] and the standard deviation of band-pass filtered SSTA [Cobb *et al.*, 2003;
308 2013; Emile-Geay *et al.*, 2016]. In this study, we use an alternative statistical approach, involving
309 histograms and PDFs [Trenberth, 1997], which does not require continuous time series to
310 characterize changes in ENSO variability. Another advantage of using these techniques is that they
311 eliminate the need to identify discrete ENSO events, an ongoing challenge for paleo-ENSO records
312 due to dating uncertainties [Emile-Geay *et al.*, 2013b; Hereid *et al.*, 2013b; Comboul *et al.*, 2014].
313 Instead, we characterize variability based on the distribution of observations over a time interval,
314 an approach analogous to the analysis of individual foraminifera preserved in marine sediment
315 [Thirumalai *et al.*, 2013], albeit with more accurate annual chronology.

316
317 The time series (Figure 2a) and histogram (Figure 2b) of Niño 3.4 monthly SST values [Rayner *et*
318 *al.*, 2003] include the total variability in the SST record, including annual, interannual, as well as
319 decadal and longer timescales. We note that for shorter records, linear or non-linear detrending
320 could be used in lieu of a high-pass filter to isolate interannual (sub-decadal) variability. SSTs in
321 the Niño 3.4 region document interdecadal variability in both the frequency and magnitude of
322 ENSO events during the instrumental record, with an increase of extreme events over the last 40
323 years [Trenberth and Hoar, 1996]. For example, the 1982-83 and 1997-98 El Niño events (Figure
324 2c) are two out of the three most extreme ENSO events on record [Santoso *et al.*, 2017]. We
325 quantify changes in ENSO variability during the 20th century using two statistical metrics
326 computed in moving windows (Figure 2e). Both the ± 2 standard deviation range ($\pm 2\sigma$) (Figure
327 2e, dashed line) as well as the difference between the 2.5 ($p_{2.5}$) and 97.5 ($p_{97.5}$) percentiles (Figure
328 2e, solid line) show lower values during the early 20th century, and higher values during the late
329 20th century that correspond with changes in the magnitude and/or frequency of ENSO events, i.e.
330 a change in ENSO variability. We note that if the data are normally distributed (Gaussian), the $p_{2.5}$
331 to $p_{97.5}$ interpercentile range is approximately equal to the ± 2 standard deviation range.

332
333 These 20th century changes in ENSO variability observed in the time domain (Figure 2e) are also
334 captured using a probabilistic framework. We target intervals of enhanced and suppressed ENSO
335 variability [Wittenberg, 2009] as end-members to demonstrate that histogram width quantifies
336 changes in variability (Figure 2f). Extreme ENSO events yield SST anomalies that fall into the
337 tails of the SSTA distribution as defined by the 2.5 and 97.5 percentiles (Figure 2d). A change in
338 ENSO variability will correspondingly increase or decrease the $p_{2.5}$ to $p_{97.5}$ interpercentile range
339 (herein referred to as the width of the distribution). The increase in ENSO variability during the
340 late 20th century extends the overall width of the SSTA PDF (Figure 2f, red PDF) as compared to
341 the interval with less ENSO variability (Figure 2f, blue PDF). Although both negative (La Niña)
342 and positive (El Niño) SST anomalies become more extreme with increased ENSO variability, the
343 relative increase in El Niño-related positive SST anomalies is larger, corroborating documented
344 [Trenberth, 1997] increases in the magnitude and frequency of strong El Niño events during the
345 late 20th century, i.e. an increase in skewness.

346
 347
 348
 349
 350
 351
 352

The distribution of SST anomalies from the Niño 3.4 region demonstrates that histograms and PDFs quantify interdecadal changes in ENSO variability during the 20th century. Although we use a continuous time series as demonstration, the histogram and PDF technique advantageously does not require long and/or continuous climate records. We subsequently apply the same statistical techniques to replicated SST records developed from modern and fossil corals from the tropical southwest Pacific.



353
 354
 355
 356
 357
 358
 359
 360
 361
 362
 363
 364
 365
 366
 367

Figure 2. Quantifying 20th century SST variability in the Niño 3.4 region. **a** Instrumental monthly SST [Rayner *et al.*, 2003] averaged over the Niño 3.4 region for 1900-2005 CE. **b** Histogram (red) and probability density function (PDF) estimate (black) of the monthly SST for 1900-2005 CE. **c** Time series of monthly SSTA. Horizontal gray lines demarcate the 2.5 and 97.5 percentiles ($p_{2.5}$, $p_{97.5}$) of the monthly SSTA over the 1900-2005 CE interval. Red triangles indicate historical El Niño events, blue triangles indicate La Niña events based on the Oceanic Niño index (NOAA, Section 3.1) and the extended multivariate ENSO index [Wolter and Timlin, 2011]. The selected ENSO events used to make the composite maps in Figure 1 are the triangles outlined in black. **d** Histogram (red, bin = 0.5°C) and PDF estimate (black) of the monthly SSTA for 1900-2005 CE. **e** The $\pm 2\sigma$ range (dashed) and $p_{97.5} - p_{2.5}$ interpercentile range (solid) computed in 20-year moving windows. **f** PDF estimates of SSTA for intervals with less (blue: 1920-1939 CE) and more (red: 1980-1999 CE) ENSO variability. Blue (red) shading in (c, e) highlight the intervals in f with less (more) ENSO variability. Numerical values above the PDFs in (d, f) denote the 2.5 and 97.5 percentiles for the designated subset interval. The horizontal bars above the PDFs in (d, f) indicate the $p_{97.5} - p_{2.5}$ interpercentile range. Monthly SSTA calculated using the same methodology as Figure 1 (Section 3.3). PDFs in this and all subsequent figures are based on a kernel density estimation method [Parzen, 1962].

368
 369
 370

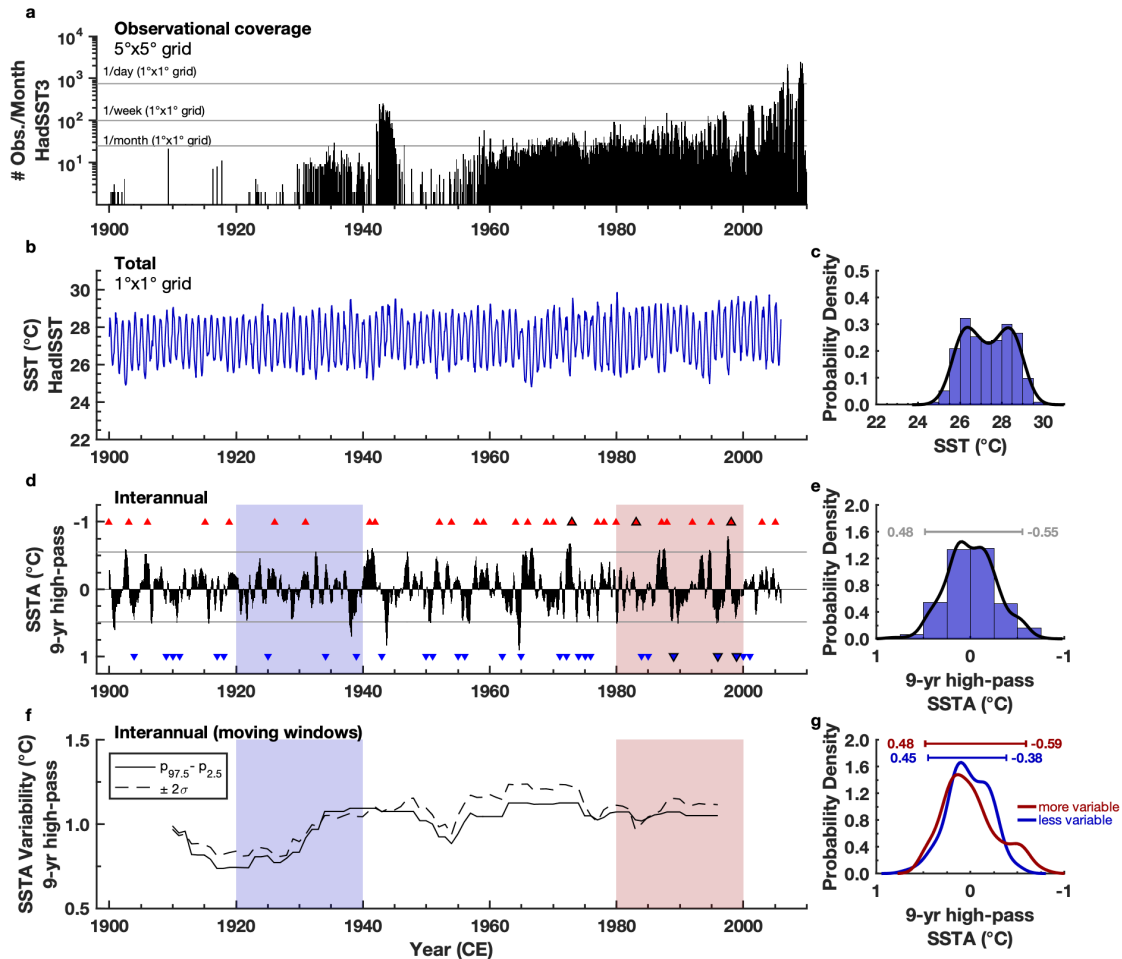
5 Results

5.1 Modern SST Variability in the Southwest Pacific (Vanuatu)

371 While it is common practice to use instrumental observations to characterize modern SST
372 variability, observational coverage [Deser *et al.*, 2010] in the southwest Pacific is limited in the
373 first half of the 20th century (Figure 3a), which leads to uncertainty in the magnitude of changes in
374 ENSO-related SST variability. The SSTA signal in the observational product at Vanuatu (Figure
375 3d) is smaller compared to the Niño 3.4 region, but Vanuatu expectedly cools and warms during
376 known historical ENSO events (Figure 1, Figure 3d). However, instrumental SSTA at Vanuatu
377 does not document a clear difference in interdecadal ENSO variability (Figure 3f) as observed in
378 the Niño 3.4 region (Figure 2e). The PDF of instrumental monthly SSTA (Figure 3g) for Vanuatu
379 shows an increase in width during the late 20th century interval; however, the difference between
380 the more and less variable intervals is small and not statistically significant (Section 3.4). The
381 SSTA distributions (Figures 3e, 3g) have a large concentration of weak anomalies, and the lack of
382 interdecadal changes in ENSO variability is most likely due to the statistical infilling of the
383 climatological mean SST when observations are lacking [Reynolds and Smith, 1994; Rayner *et al.*,
384 2003] (Figure 3a). Given a documented lack of variability in gridded SST products for observation-
385 limited regions [Rayner *et al.*, 2003], our modern coral-based SST reconstruction augments limited
386 SST products and demonstrates the need for additional modern coral climate records from data-
387 sparse regions.

388
389 The coral skeleton used to reconstruct and characterize modern monthly SST variability in the
390 southwest Pacific was collected from a live *P. lutea* coral head at 8 m water depth at Sabine Bank,
391 Vanuatu during a trip in 2006 [Gorman *et al.*, 2012] (15.9°S, 166.0°E; Section 2.1). We apply the
392 same analytical techniques used for instrumental SST to SST derived from coral Sr/Ca (Figure 4a)
393 to test how corals from the southwest Pacific record changes in ENSO variability.

394
395 The Sabine Bank modern coral Sr/Ca-SSTA reconstruction (Figure 4, Figure S2) faithfully
396 captures known interdecadal changes in ENSO variability over the last 100 years, as observed in
397 the Niño 3.4 region. The SSTA estimates from the corals, which are a point source, are larger than
398 that for the spatially interpolated instrumental SST product (Figure 3d), but importantly, the coral
399 reconstruction agrees with the instrumental data that individual historical ENSO events alter SST
400 in the region (Figure 4c). Another notable distinction is that unlike instrumental SST, the SSTA
401 reconstruction from the coral archive faithfully captures known interdecadal changes in
402 interannual variability over the 20th century (Figure 4e). Reconstructed interannual SST variability
403 at Vanuatu (Figure 4e) tracks the pattern of lower variability during the early 20th century and a
404 late 20th century increase in variability as observed in the Niño 3.4 region (Figure 2e). This change
405 is also captured by the PDFs for the select intervals with more and less ENSO variability (Figure
406 4f). La Niña-related positive excursions become more extreme during the interval with enhanced
407 ENSO variability (Figure 4f; $p_{97.5}$ less variable/more variable: 0.63 vs. 1.00 °C). El Niño-related
408 negative SST anomalies also become more extreme ($p_{2.5}$ less variable/more variable: -0.83 vs. -
409 1.26 °C). The larger values for the variability metrics in moving windows (Figure 4e) in
410 conjunction with the increased width of the SSTA distribution for the interval with more ENSO
411 variability (Figure 4f, red PDF) demonstrate that southwest Pacific modern coral Sr/Ca-SST
412 captures the changes in ENSO variability observed in instrumental SST for the Niño 3.4 region
413 (Figure 2e, 2f).



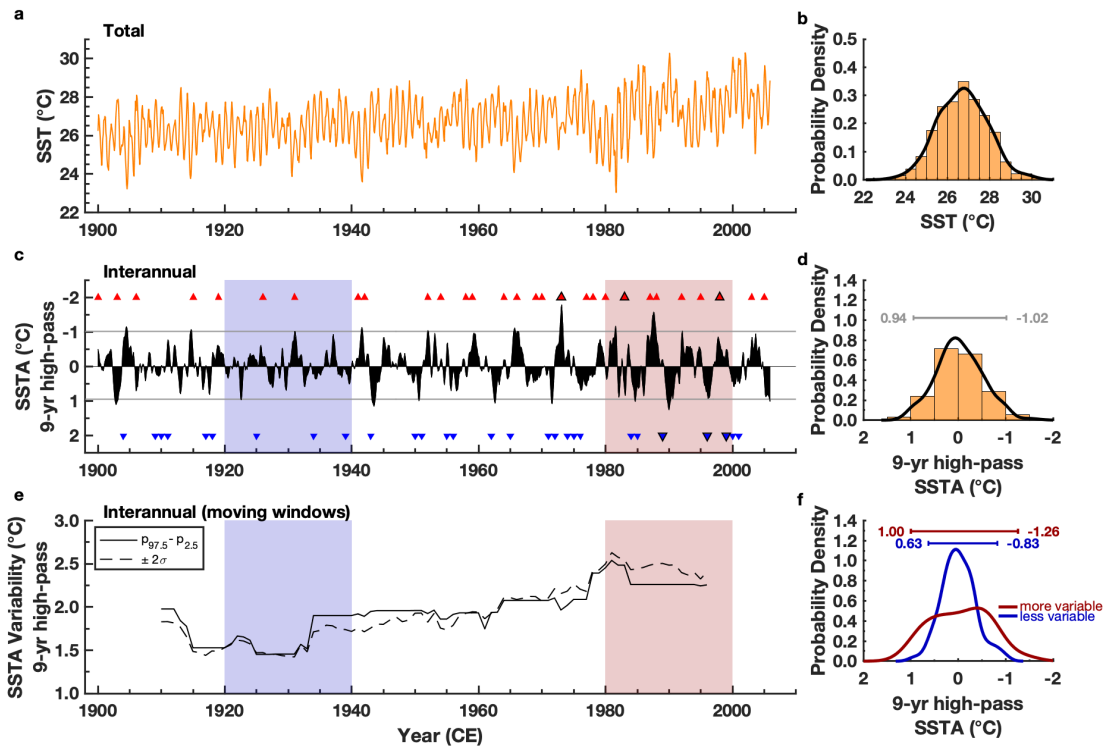
414 **Figure 3. Quantifying 20th century instrumental SST variability at Vanuatu (SW Pacific).** The number of
 415 observations per month in the 5° latitude x 5° longitude HadSST3 [Kennedy *et al.*, 2011a; 2011b] grid box (17.5°S,
 416 167.5°E) that includes Vanuatu. Note the logarithmic scale for the number of observations per month and the
 417 horizontal gray lines that indicate the number of observations required to achieve specified temporal coverages. The
 418 amplitude of SST variability outside of the monthly mean-removed climatology is loosely tied to the number of
 419 observations, such that more observations lead to more interannual, and even decadal, SST variability. **b** Instrumental
 420 monthly SST [Rayner *et al.*, 2003] and **c** the histogram (blue, bin = 0.5 °C) and PDF (black) of monthly SST for
 421 Vanuatu. The SST data are the average of the two grid points closest to the coral sites (15.5°S, 166.5°E) and (16.5°S,
 422 166.5°E; Section 3.1). **d** Instrumental monthly SSTA. Horizontal gray lines demarcate the $p_{2.5}$ and $p_{97.5}$ monthly SSTA
 423 values for the 1900–2005 CE interval. Red triangles indicate El Niño events and blue triangles indicate La Niña events
 424 as in Fig. 2c. **e** Histogram (blue, bins = 0.5 °C) and PDF (black) of monthly SSTA for the 1900–2005 CE interval. **f**
 425 The $\pm 2\sigma$ range (dashed) and $p_{97.5} - p_{2.5}$ interpercentile range (solid) of monthly SSTA computed in 20-year moving
 426 windows. **g** PDF estimates of monthly SSTA for intervals with less (blue: 1920–1939 CE) and more (red: 1980–1999
 427 CE) ENSO variability observed in the Niño 3.4 region (Fig. 2). Monthly SSTA computed the same as Fig. 1 (Section
 428 3.3). The numerical values and horizontal bar above the PDF in **e**, **g** indicate the $\sim \pm 2\sigma$ range as defined by the
 429 percentiles.
 430

431
 432 Our uncertainty quantification explores whether the Sr/Ca estimates of SST result in larger changes
 433 compared to instrumental data, and whether the changes in ENSO variability are statistically
 434 significant. The reported uncertainty in the 2.5 and 97.5 percentiles for modern coral SSTA is

435 ± 0.21 °C for the monthly SSTA (Figure 4d, 4f) based on a Monte Carlo error propagation
436 algorithm with analytical, calibration, and replication uncertainties [Thirumalai *et al.*, 2014]
437 (Figure S4, Section 3.4). Replication of the coral records quantifies the term that we refer to as
438 “geological” uncertainty, which is due to all other sources, including the oceanographic and
439 geologic setting, sampling, etc. We quantify this geological uncertainty by comparing two modern
440 corals over a common interval (1941-1990 CE) from the southwest Pacific (Section 3.4). Our
441 second, replication coral comes from Malo Channel, Vanuatu [Kilbourne *et al.*, 2004] (15.7°S,
442 167.2°E), ~120 km to the northeast of Sabine Bank.

443
444 The $\pm 2\sigma$ range for the Sabine Bank modern coral SSTA distribution (1941-1990 replication
445 interval) is ± 0.16 °C including analytical and calibration uncertainty (Figure S4). The $\pm 2\sigma$ range
446 for the Malo Channel modern coral SSTA distribution (1941-1990 replication interval) is ± 0.14
447 °C including analytical and calibration uncertainty. The resultant root mean square error is thus
448 ± 0.21 °C as reported above. The modern coral SSTA distributions (Figure 6a) are reproducible
449 over their common period of overlap and come from the same continuous distribution (passes the
450 K-S test [Frank J Massey, 1951] at the 1% significance level regardless of the effective degrees of
451 freedom; Section 3.4). The intervals of more and less ENSO activity reconstructed from the Sabine
452 Bank modern coral SSTA (Figure 4f) are significantly different at an effective degree of freedom
453 65.8% less ($v_{\text{eff}} = 82$) than the total number of months in each interval ($n = 240$; Section 3.4).

454
455 We further explored the fidelity of the differences in the $p_{2.5}$ and $p_{97.5}$ values taking the total
456 uncertainty into account. We used the results from our uncertainty analysis (Figure S4) to examine
457 the overlap between the $p_{2.5}$ and $p_{97.5}$ distributions for the intervals with more and less ENSO
458 variability (Figure S5). The amount of overlap between two percentile distributions highlights the
459 similarity or difference between the reported percentile values. Our analysis confirms that the
460 known changes in 20th century ENSO variability are recorded by corals from the southwest Pacific,
461 that the estimates are larger than instrumental estimates of SST changes, and that the changes in
462 ENSO variability are large compared to the calculated uncertainty of the coral-based SSTA
463 reconstruction.



464
 465 **Figure 4. Quantifying 20th century SST variability in the SW Pacific using modern corals.** **a** Reconstructed
 466 monthly SST based on modern coral Sr/Ca from Sabine Bank, Vanuatu (15.9°S, 166.0°E). Monthly SST (total
 467 variability) shows a shift toward warmer SST due to a late 20th century warming trend in the coral Sr/Ca time series.
 468 **b** Histogram (orange, bin = 0.5 °C) and PDF (black) of monthly SST over the 1900-2005 CE interval. **c** Coral-based
 469 monthly SSTA. Horizontal gray lines demarcate the $p_{2.5}$ and $p_{97.5}$ monthly SSTA values for the 1900-2005 CE interval.
 470 Red triangles indicate El Niño events and blue triangles indicate La Niña events as in Fig. 2c. **d** Histogram (orange,
 471 bins = 0.5 °C) of monthly SSTA for 1900-2005 CE. **e** The $\pm 2\sigma$ range (dashed) and $p_{97.5} - p_{2.5}$ interpercentile range
 472 (solid) of monthly SSTA computed in 20-year moving windows. **f** PDF estimates of monthly SSTA for the intervals
 473 with less (blue: 1920-1939 CE) and more (red: 1980-1999 CE) ENSO variability observed in the Niño 3.4 region (Fig.
 474 2). The numerical values and horizontal bar above the PDFs in **d**, **f** indicate the $\sim \pm 2\sigma$ range as defined by the 2.5 and
 475 97.5 percentiles. Blue (red) shading in **(c, e)** highlight the intervals in **f** with less (more) ENSO variability (Fig. 2).
 476 Monthly SSTA computed the same as Fig. 1 (Section 3.3). The uncertainty in the 2.5 and 97.5 percentiles in **(d, f)** is
 477 ± 0.21 °C based on analytical, calibration, and replication uncertainties (Section 3.4).
 478

479 5.2 Medieval Climate Anomaly SST Variability in the Southwest Pacific (Vanuatu)

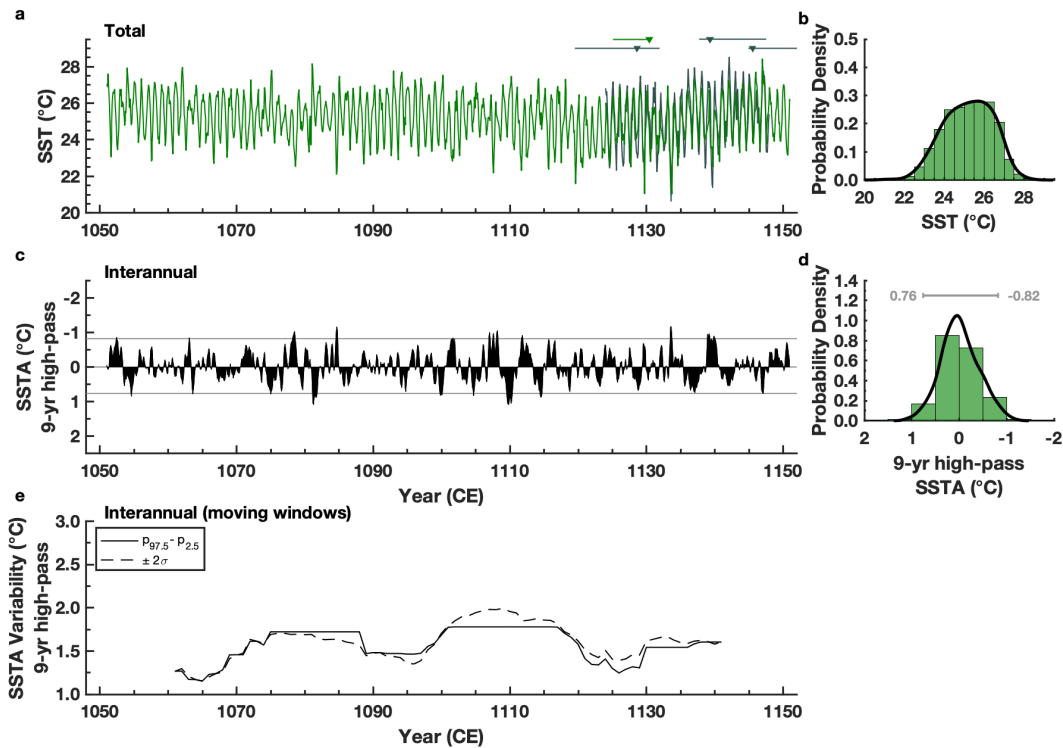
480
 481 After demonstrating that modern corals from the southwest Pacific capture observed changes in
 482 ENSO variability, we next apply our statistical approach to corals from the MCA. The tectonic
 483 activity at Tasmaloum, Vanuatu (15.6°S, 166.9°E) yields pristine, well-preserved *in situ* fossil
 484 coral heads above present-day sea level. Our cores are collected from an uplifted reef, so we have
 485 the unique opportunity to sample multiple, contemporaneous coral heads and quantify the
 486 uncertainty in our fossil coral climate reconstruction via replication. The monthly SST anomalies
 487 for both fossil corals are calculated with respect to the 1126-1145 CE climatology since this
 488 interval is common to both corals. High precision U-Th dating [Shen *et al.*, 2012; Cheng *et al.*,
 489 2013] confirms that the century-long fossil coral 11-TM-S5 (^{230}Th age: 1127.1 ± 2.7 CE, 2σ
 490 analytical uncertainty) and the shorter, 24-year-long replication coral 11-TM-I1 (^{230}Th ages:

491 1125.7 ± 6.2, 1142.6 ± 4.9, 1149.0 ± 4.1 CE, 2σ analytical uncertainty) selected for this study were
492 alive ~900 years ago during the MCA (Section 2.1; Table S1).

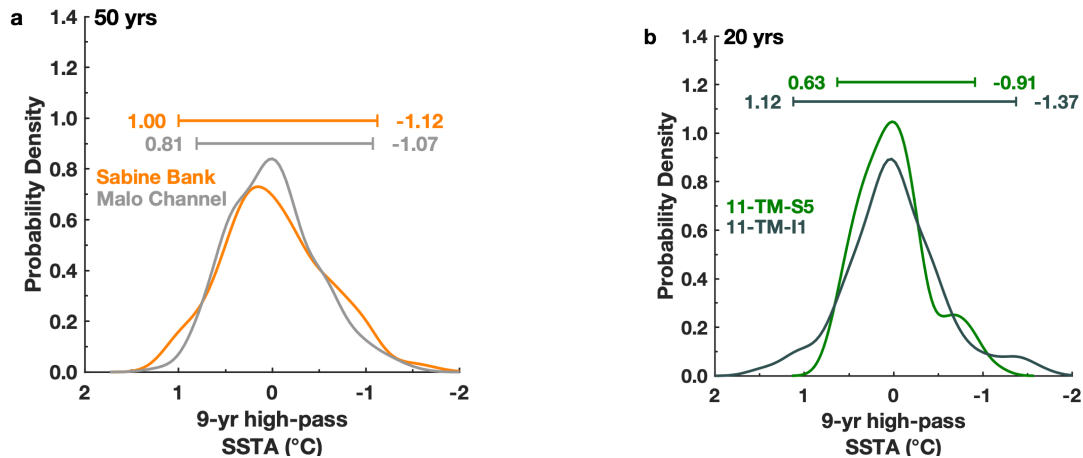
493
494 We apply our statistical techniques to the SST record derived from fossil coral Sr/Ca (Figure 5a)
495 as a test of ENSO variability during a century of the MCA (1051–1150 CE). The MCA fossil coral
496 SST (Figure 5a) encompasses the total variability in the record and shows similar overall
497 variability (Figure 5b) compared to the modern period (Figure 4b). The SSTA time series (Figure
498 5c) shows both positive and negative excursions that correspond to ENSO events. However, the
499 number of large SSTA excursions is smaller and leads to a narrower SSTA distribution (Figure
500 5d). While the modern SSTA shows a unidirectional increase in ENSO variability from the early
501 to late 20th century (Figure 4e), interannual SST variability during the MCA fluctuates between
502 intervals with more and less variability (Figure 5e). For example, 1070-1090 CE has more
503 interannual variability, while 1120-1140 CE has less variability as quantified by the ±2σ and
504 interpercentile ranges. However, neither variability metric for the MCA (Figure 5e) exceeds the
505 values for the last two decades of the 20th century (Figure 4e).

506
507 We can compare the SSTA distribution for the MCA (Figure 5d) to either a century of modern
508 coral data (Figure 4d) or discrete windows of time in the modern era (Figure 4f). The values for
509 ENSO variability, as quantified by the percentiles of the SSTA distribution (Figure 5d), are 0.76
510 °C for La Niña-related SSTA (p_{97.5}) and -0.82 °C for El Niño-related SSTA (p_{2.5}), similar to what
511 we observe during the earlier part of the 20th century (Figure 4f). We choose to show an entire
512 century of data but note that our results are consistent if we choose a subset of the fossil coral time
513 series and generate the PDFs in 20-year moving windows (Figure S8).

514
515 The populations of SSTA for the two MCA fossil corals (Figure 6b) are drawn from the same
516 distribution over their common interval of overlap, as they pass the K-S test [*Frank J Massey*,
517 1951] at the 1% significance level (regardless of the effective degrees of freedom; Section 3.4).
518 The uncertainty in extreme monthly SSTA values (Figure 5d, 2.5 and 97.5 percentiles) is ±0.24
519 °C based on our algorithm with analytical, calibration and geological uncertainty (Section 3.4).
520 Incorporating the total uncertainty, we find that ENSO variability during the MCA, as recorded by
521 the fossil corals, is within the range of ENSO variability observed in the modern and is
522 significantly different than the interval with more ENSO variability during the late 20th century
523 (Figure S6). Moreover, we cannot distinguish the SSTA population that records ENSO variability
524 during the MCA as significantly different than the modern interval with less ENSO variability
525 (based on K-S tests [*Frank J Massey*, 1951] at the 1% significance level and Figure S7). However,
526 we can distinguish the SSTA population during the MCA as significantly different than the SSTA
527 population during modern interval with more ENSO variability (via the K-S test), and the new
528 coral records from Vanuatu show less ENSO variability during the MCA as compared to the late
529 20th century.

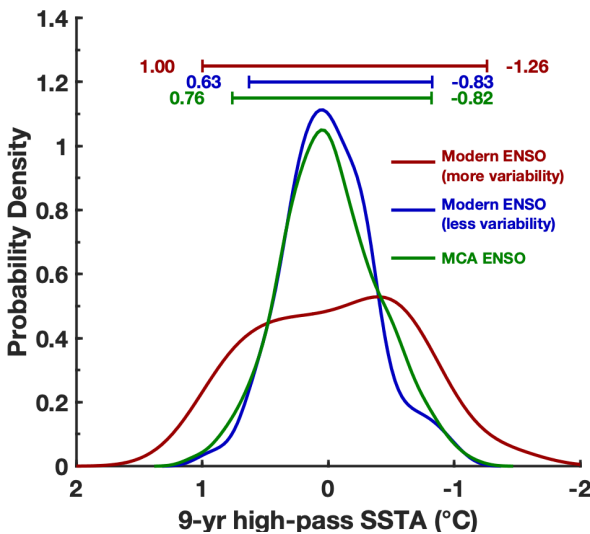


531
 532 **Figure 5. Quantifying Medieval Climate Anomaly SST variability in the SW Pacific using fossil corals.** **a**
 533 Reconstructed monthly SST based on fossil coral Sr/Ca from Tasmaloum, Vanuatu (15.6°S, 166.9°E). Coral 11-TM-
 534 S5 (green; $^{230}\text{Th} \pm 2\sigma$ age: 1127.1 ± 2.7 CE) and 11-TM-I1 (gray; $^{230}\text{Th} \pm 2\sigma$ ages: 1125.7 ± 6.2 , 1142.6 ± 4.9 , 1149.0
 535 ± 4.1 CE). Triangles with horizontal bars mark the ^{230}Th ages and $\pm 2\sigma$ analytical error (see Section 2.3 for a description
 536 of the fossil coral alignment). **b** Histogram (green, bin = 0.5 °C) and PDF (black) of monthly SST over the 1051-1150
 537 CE interval. **c** Coral-based monthly SSTA. Horizontal gray lines demarcate the $p_{2.5}$ and $p_{97.5}$ monthly SSTA values
 538 for the 1051-1150 CE interval. **d** Histogram (green, bins = 0.5 °C) of monthly SSTA for the 1051-1150 CE interval.
 539 **e** The $\pm 2\sigma$ range (dashed) and $p_{97.5} - p_{2.5}$ interpercentile range (solid) of monthly SSTA computed in 20-year moving
 540 windows. The numerical values and horizontal bar above the PDF in **d** indicate the $\sim \pm 2\sigma$ range as defined by the 2.5
 541 and 97.5 percentiles. Monthly SSTA computed the same as Fig. 1 (Section 3.3). The uncertainty in the 2.5 and 97.5
 542 percentiles in (**d**, **f**) is ± 0.24 °C based on analytical, calibration, and replication uncertainties (Section 3.4).



543
544
545
546
547
548
549
550
551
552
553

Figure 6. Modern and MCA fossil coral SSTA replication. PDFs of monthly SSTA for the modern and MCA corals over their respective common intervals of overlap. **a** Replication results for 50 years (1941-1990 CE) of modern monthly SSTA data. PDF estimates for Sabine Bank (orange) and Malo Channel [Kilbourne *et al.*, 2004] (gray), Vanuatu. **b** Replication results for 20 years (1126-1145 CE) of MCA fossil coral monthly SSTA data from Tasmaloum, Vanuatu. 11-TM-S5 (green) and 11-TM-I1 (gray). Monthly SSTA computed the same as Fig. 1 (Section 3.3). Numerical values and horizontal bars above the PDFs in **a**, **b** indicate $\sim \pm 2\sigma$ range as defined by the 2.5 and 97.5 percentiles. The uncertainty in the 2.5 and 97.5 percentiles is ± 0.21 °C (**a**) and ± 0.24 °C (**b**) based on analytical, calibration, and replication uncertainties (Section 3.4).



554
555
556
557
558
559
560
561

Figure 7. Coral-based ENSO variability comparison: Modern vs. MCA. PDF estimates of monthly SSTA (reconstructed from SW Pacific coral Sr/Ca) for the more (red) and less (blue) variable ENSO intervals during the 20th century (from Fig. 4f) and 100 years during the MCA (green; from Fig. 5d). Numerical values and horizontal bars above the PDFs indicate $\sim \pm 2\sigma$ range as defined by the 2.5 and 97.5 percentiles. The uncertainty in the 2.5 and 97.5 percentiles is ± 0.21 °C (modern) and ± 0.24 °C (MCA) based on analytical, calibration, and replication uncertainties (Section 3.4).

562 6 Discussion and Conclusions

563 Previously published proxy records of ENSO [Moy *et al.*, 2002; Cobb *et al.*, 2003; Rein *et al.*,
564 2004; Newton *et al.*, 2006; Rustic *et al.*, 2015] for the MCA and the Little Ice Age (LIA: 1450-

565 1850 CE [*Masson-Delmotte et al.*, 2013]) often show conflicting results, indicating large
566 uncertainties in the proxy records, in our estimations of the range of natural variability, or both.
567 Numerous records provide evidence for a strengthened SST gradient across the equatorial Pacific
568 and/or an inferred reduction in ENSO variability during the MCA relative to the LIA [*Cobb et al.*,
569 2003; *Newton et al.*, 2006; *Rustic et al.*, 2015]. In contrast, other proxy records [*Moy et al.*, 2002;
570 *Rein et al.*, 2004] indicate a peak in ENSO variability during the MCA. Two recent compilations
571 of ENSO-sensitive records actually find no statistically significant change in ENSO variability
572 between the MCA and the LIA and highlight the need for additional high-resolution proxy records
573 to fully characterize the range of ENSO variability over the Common Era [*Emile-Geay et al.*,
574 2013b; *Henke et al.*, 2017].

575
576 Internal climate variability contributes a large source of uncertainty in detecting forced changes in
577 ENSO variability over the Common Era. Our results show a prolonged period of low variability
578 during a time with external forcings similar to pre-industrial values [*Bradley et al.*, 2016]. We
579 interpret our results in tandem with the compilation studies to indicate that devoid of strong
580 external climate forcing, internal variability within the climate system can produce a wide range
581 of responses in the variability of ENSO. The PDF for coral data from the MCA indicates that
582 ENSO variability over a full century is statistically indistinguishable from two decades with less
583 ENSO variability observed during the 20th century (Figure 7, Figure S7). Furthermore, even when
584 including the total uncertainty in the coral reconstructions ($\pm 2\sigma$ analytical, calibration, and
585 geological uncertainty), ENSO variability during the MCA and the early 20th century is statistically
586 different and lower than the recent decades with larger ENSO variability (Figures S5 and S6).
587 Thus, we conclude that while the MCA contained lower ENSO variability, such ranges have been
588 observed in the historical record.

589
590 Although our study focuses on ENSO variability during the Common Era, the histogram and PDF
591 technique we present here is broadly applicable to other paleoclimate studies that seek to
592 reconstruct variability across a variety of timescales. Quantifying the range of natural variability
593 is critical as it may complicate our ability to detect a forced ENSO response from short records
594 during times with different background states such as the mid-Holocene, the Last Glacial
595 Maximum, future climate scenarios, and the most recent decades of instrumental data. Only by
596 collecting more paleoclimate proxy data can we establish a baseline to determine if changes in
597 ENSO variability during these other times are outside the bounds of natural variability. Our
598 findings provide new insight to this challenge by replicating the bounds of low ENSO variability
599 from two different time periods, and showing that intervals of low ENSO variability can last for a
600 full century, consistent with multi-decadal to centennial intervals of reduced ENSO variability
601 simulated in unforced climate models [*Wittenberg*, 2009; *Deser et al.*, 2012].

602 603 **Acknowledgements**

604
605 This research was supported by the National Science Foundation (OCE-1103430 to T.M.Q) and
606 the National Science Foundation Graduate Research Fellowship Program (to A.E.L). This study
607 was also partially supported by grants from the Science Vanguard Research Program of the
608 Ministry of Science and Technology (MOST) (107-2119-M-002-051 to C.-C.S.), the National
609 Taiwan University (105R7625 to C.-C.S), and the Higher Education Sprout Project of the Ministry
610 of Education, Taiwan ROC (107L901001 to C.-C.S.), and Brown University (Presidential

611 Postdoctoral Fellowship to K.T.). We thank Pedro DiNezio, Charles Jackson, Yuko Okumura, and
612 Tim Shanahan for their review of the analysis and uncertainty quantification. We thank Elizabeth
613 Dunn and Chris Maupin for their involvement with the initial sampling of the modern coral from
614 Sabine Bank. We thank the captain and crew of the IRD vessel R/V *Alis*, Guy Cabioch, James
615 Austin, Bernard Pelletier, Valérie Ballu, Christophe Maes, and Steffen Sastrup for their assistance
616 with the drilling operations at Sabine Bank, Vanuatu. We also acknowledge Esline Garaebiti-Bule
617 and Douglas Charley of the Geohazards Unit of the Geology and Mines Department of the
618 Republic of Vanuatu, Joel Path, Secretary General of SANMA Province, Republic of Vanuatu,
619 and Edwin Tae for supporting our projects. We thank Tom Crowley for his early support and
620 motivation for fossil coral work in the southwest Pacific.

621

622 **Author Contributions**

623

624 A.E.L wrote the manuscript, sampled the fossil corals, and performed all the fossil coral Sr/Ca
625 analyses. A.E.L performed the data analysis and interpreted the results with T.M.Q and J.W.P.
626 K.T. assisted with the data analysis and uncertainty quantification. F.W.T. drilled the modern
627 coral, and F.W.T and J.W.P drilled the fossil coral samples with support from T.M.Q. M.K.G.
628 sampled the modern coral from Sabine Bank, Vanuatu and generated the original modern coral
629 Sr/Ca data composite. C.-C.S, C.-C.W, and T.-L.Y provided the ^{230}Th ages for the fossil corals.
630 All authors reviewed the manuscript.

631

632 **Data Availability**

633

634 All coral Sr/Ca data from Sabine Bank and Tasmaloum, Vanuatu produced from this study will be
635 archived in the paleoclimatology dataset repository in the National Centers for Environmental
636 Information, NOAA database upon publication ([https://www.ncdc.noaa.gov/data-
637 access/paleoclimatology-data/datasets](https://www.ncdc.noaa.gov/data-access/paleoclimatology-data/datasets)).

638

639 **Code Availability**

640

641 The MATLAB codes that have contributed to the analysis and results in this study are available
642 upon request from the lead author (A.E.L: alawman@utexas.edu).

643

644 **Additional Information**

645

646 **Supporting information** is available for this paper.

647

648 **Competing Financial Interests:** The authors declare no competing financial interests.

649

650 **Correspondence and requests for materials** should be addressed to A.E.L.

651 **References**

652 Ballu, V., P. Bonnefond, S. Calmant, M. N. Bouin, B. Pelletier, O. Laurain, W. C. Crawford, C.
653 Baillard, and O. de Viron (2013), Using altimetry and seafloor pressure data to estimate
654 vertical deformation offshore: Vanuatu case study, *Adv. Space Res.*, 51(8), 1335–1351,
655 doi:10.1016/j.asr.2012.06.009.

- 656 Bard, E., G. Raisbeck, F. Yiou, and J. Jouzel (2000), Solar irradiance during the last 1200 years
657 based on cosmogenic nuclides, *Tellus*, 52B, 985–992, doi:10.3402/tellusb.v52i3.17080.
- 658 Bertrand, C., M. F. Loutre, M. Crucifix, and A. Berger (2002), Climate of the last millennium: A
659 sensitivity study, *Paleoceanography*, 52A, 221–244, doi:10.1034/j.1600-0870.2002.00287.x.
- 660 Bjerknes, J. (1969), Atmospheric teleconnections from the equatorial pacific, *Mon. Weather*
661 *Rev.*, 97(3), 163–172, doi:10.1175/1520-0493(1969)097<0163:ATFTEP>2.3.CO;2.
- 662 Bradley, R. S., H. Wanner, and H. F. Diaz (2016), The Medieval Quiet Period, *The Holocene*,
663 26(6), 990–993, doi:10.1177/0959683615622552.
- 664 Cheng, H. et al. (2013), Improvements in ^{230}Th dating, ^{230}Th and ^{234}U half-life values, and U–Th
665 isotopic measurements by multi-collector inductively coupled plasma mass spectrometry,
666 *Earth Planet. Sci. Lett.*, 371–372(C), 82–91, doi:10.1016/j.epsl.2013.04.006.
- 667 Cobb, K. M., C. D. Charles, H. Cheng, and R. E. Nature (2003), El Niño/Southern Oscillation
668 and tropical Pacific climate during the last millennium, *Nature*, 424(6946), 271–276,
669 doi:10.1038/nature01779.
- 670 Cobb, K. M., N. Westphal, H. R. Sayani, J. T. Watson, E. Di Lorenzo, H. Cheng, R. L. Edwards,
671 and C. D. Charles (2013), Highly variable El Niño–Southern Oscillation throughout the
672 Holocene, *Science*, 339(6115), 67–70, doi:10.1126/science.1228246.
- 673 Collins, M. et al. (2010), The impact of global warming on the tropical Pacific Ocean and El
674 Niño, *Nature Geosci.*, 3(6), 391–397, doi:10.1038/ngeo868.
- 675 Comboul, M., J. Emile-Geay, M. N. Evans, N. Mirnateghi, K. M. Cobb, and D. M. Thompson
676 (2014), A probabilistic model of chronological errors in layer-counted climate proxies:
677 applications to annually banded coral archives, *Clim. Past*, 10(2), 825–841, doi:10.5194/cp-
678 10-825-2014.
- 679 Corrège, T. (2006), Sea surface temperature and salinity reconstruction from coral geochemical
680 tracers, *Palaeogeogr. Palaeoclimatol. Palaeoecol.*, 232(2-4), 408–428,
681 doi:10.1016/j.palaeo.2005.10.014.
- 682 Cravatte, S., T. Delcroix, D. Zhang, M. McPhaden, and J. Leloup (2009), Observed freshening
683 and warming of the western Pacific Warm Pool, *Clim Dyn*, 33(4), 565–589,
684 doi:10.1007/s00382-009-0526-7.
- 685 Crowley, T. J. (2000), Causes of climate change over the past 1000 Years, *Science*, 289(5477),
686 270–277, doi:10.1126/science.289.5477.270.
- 687 DeLong, K. L., T. M. Quinn, C.-C. Shen, and K. Lin (2010), A snapshot of climate variability at
688 Tahiti at 9.5 ka using a fossil coral from IODP Expedition 310, *Geochem. Geophys.*
689 *Geosyst.*, 11(6), doi:10.1029/2009GC002758.

- 690 DeLong, K. L., T. M. Quinn, F. W. Taylor, C.-C. Shen, and K. Lin (2013), Improving coral-base
691 paleoclimate reconstructions by replicating 350 years of coral Sr/Ca variations, *Palaeogeogr.*
692 *Palaeoclimatol. Palaeoecol.*, 373(C), 6–24, doi:10.1016/j.palaeo.2012.08.019.
- 693 Deser, C., A. S. Phillips, R. A. Tomas, Y. Okumura, M. A. Alexander, A. Capotondi, J. D. Scott,
694 Y.-O. Kwon, and M. Ohba (2012), ENSO and Pacific decadal variability in the Community
695 Climate System Model version 4, *J. Clim.*, 25, 2622–2651, doi:10.1175/JCLI-D-11-00301.1.
- 696 Deser, C., M. A. Alexander, S.-P. Xie, and A. S. Phillips (2010), Sea surface temperature
697 variability: Patterns and mechanisms, *Annu. Rev. Marine. Sci.*, 2(1), 115–143,
698 doi:10.1146/annurev-marine-120408-151453.
- 699 DiNezio, P. N., G. A. Vecchi, and A. C. Clement (2013), Detectability of changes in the Walker
700 circulation in response to global warming, *J. Climate*, 26(12), 4038–4048, doi:10.1175/JCLI-
701 D-12-00531.1.
- 702 Emile-Geay, J. et al. (2016), Links between tropical Pacific seasonal, interannual and orbital
703 variability during the Holocene, *Nature Geosci.*, 9(2), 168–173, doi:10.1038/ngeo2608.
- 704 Emile-Geay, J., K. M. Cobb, M. E. Mann, and A. T. Wittenberg (2013a), Estimating Central
705 Equatorial Pacific SST Variability over the Past Millennium. Part I: Methodology and
706 Validation, *J. Climate*, 26(7), 2302–2328, doi:10.1175/JCLI-D-11-00510.1.
- 707 Emile-Geay, J., K. M. Cobb, M. E. Mann, and A. T. Wittenberg (2013b), Estimating Central
708 Equatorial Pacific SST Variability over the Past Millennium. Part II: Reconstructions and
709 Implications, *J. Climate*, 26(7), 2329–2352, doi:10.1175/JCLI-D-11-00511.1.
- 710 Fairbanks, R. G., M. N. Evans, J. L. Rubenstone, R. A. Mortlock, K. Broad, M. D. Moore, and
711 C. D. Charles (1997), Evaluating climate indices and their geochemical proxies measured in
712 corals, *Coral Reefs*, 16(1), S93–S100, doi:10.1007/s003380050245.
- 713 Frank J Massey, S. J. S. (1951), The Kolmogorov-Smirnov test for goodness of fit, *J. Am. Stat.*
714 *Assoc.*, 46(253), 68–78, doi:10.2307/2280095?refreqid=search-
715 gateway:b95cf3d0c48184d95f63cd76038a2f8a.
- 716 Fritsch, F. N., R. C. S. J. O. N. Analysis, 1980 (1980), Monotone piecewise cubic interpolation,
717 *SIAM*, 17(2), 238–246, doi:10.1137/0717021.
- 718 Gagan, M. K., L. K. Ayliffe, J. W. Beck, J. E. Cole, E. Druffel, R. B. Dunbar, and D. P. Schrag
719 (2000), New views of tropical paleoclimates from corals, *Quat. Sci. Rev.*, 19, 45–64,
720 doi:10.1016/S0277-3791(99)00054-2.
- 721 Gao, C., A. Robock, and C. Ammann (2008), Volcanic forcing of climate over the past 1500
722 years: An improved ice core-based index for climate models, *J. Geophys. Res.*, 113(D23),
723 D23111–15, doi:10.1029/2008JD010239.
- 724 Gorman, M. K., T. M. Quinn, F. W. Taylor, J. W. Partin, G. Cabioch, J. A. Austin Jr., B.
725 Pelletier, V. Ballu, C. Maes, and S. Saustrop (2012), A coral-based reconstruction of sea

- 726 surface salinity at Sabine Bank, Vanuatu from 1842 to 2007 CE, *Paleoceanography*, 27(3),
727 doi:10.1029/2012PA002302.
- 728 Henke, L. M. K., F. H. Lambert, and D. J. Charman (2017), Was the Little Ice Age more or less
729 El Niño-like than the Medieval Climate Anomaly? Evidence from hydrological and
730 temperature proxy data, *Clim. Past*, 13(3), 267–301, doi:10.5194/cp-13-267-2017.
- 731 Hereid, K. A., T. M. Quinn, and Y. M. Okumura (2013a), Assessing spatial variability in El
732 Niño-Southern Oscillation event detection skill using coral geochemistry,
733 *Paleoceanography*, 28(1), 14–23, doi:10.1029/2012PA002352.
- 734 Hereid, K. A., T. M. Quinn, F. W. Taylor, C. C. Shen, R. Lawrence Edwards, and H. Cheng
735 (2013b), Coral record of reduced El Niño activity in the early 15th to middle 17th centuries,
736 *Geology*, 41(1), 51–54, doi:10.1130/G33510.1.
- 737 Hu, J., J. Emile-Geay, and J. Partin (2017), Correlation-based interpretations of paleoclimate
738 data – where statistics meet past climates, *Earth Planet. Sci. Lett.*, 459, 362–371,
739 doi:10.1016/j.epsl.2016.11.048.
- 740 Kennedy, J. J., N. A. Rayner, R. O. Smith, D. E. Parker, and M. Saunby (2011a), Reassessing
741 biases and other uncertainties in sea surface temperature observations measured in situ since
742 1850: 1. Measurement and sampling uncertainties, *J. Geophys. Res.*, 116(D14), D12106–13,
743 doi:10.1029/2010JD015218.
- 744 Kennedy, J. J., N. A. Rayner, R. O. Smith, D. E. Parker, and M. Saunby (2011b), Reassessing
745 biases and other uncertainties in sea surface temperature observations measured in situ since
746 1850: 2. Biases and homogenization, *J. Geophys. Res.*, 116(D14), 1–22,
747 doi:10.1029/2010JD015220.
- 748 Kilbourne, K. H., T. M. Quinn, F. W. Taylor, T. Delcroix, and Y. Gouriou (2004), El Niño-
749 Southern Oscillation-related salinity variations recorded in the skeletal geochemistry of a
750 *Porites* coral from Espiritu Santo, Vanuatu, *Paleoceanography*, 19(4),
751 doi:10.1029/2004PA001033.
- 752 Linsley, B. K., A. Kaplan, and Y. Gouriou (2006), Tracking the extent of the South Pacific
753 Convergence Zone since the early 1600s, *Geochem. Geophys. Geosyst.*, 7,
754 doi:10.1029/2005GC001115.
- 755 Liu, Z., Z. Lu, X. Wen, B. L. Otto-Bliesner, A. Timmermann, and K. M. Cobb (2014), Evolution
756 and forcing mechanisms of El Niño over the past 21,000 years, *Nature*, 515(7528), 550–553,
757 doi:10.1038/nature13963.
- 758 Marshall, J. F., and M. T. McCulloch (2002), An assessment of the Sr/Ca ratio in shallow water
759 hermatypic corals as a proxy for sea surface temperature, *Geochim. Cosmochim. Acta*,
760 66(18), 3263–3280, doi:10.1016/S0016-7037(02)00926-2.
- 761 Masson-Delmotte, V. et al. (2013), Information from paleoclimate archives, edited by T. F.

- 762 Stocker, D. Qin, G.-K. Plattner, M. Tignor, S. K. Allen, J. Boschung, A. Nauels, Y. Xia, V.
763 Bex, and P. M. Midgley, *Climate change 2013: The Physical Science Basis. Contribution of*
764 *Working Group I to the Fifth Assessment Report of the Intergovernmental Panel on Climate*
765 *Change*, Cambridge Univ. Press, Cambridge, United Kingdom and New York, NY USA.
766
- 767 McGregor, S., A. Timmermann, M. H. England, O. Elison Timm, and A. T. Wittenberg (2013),
768 Inferred changes in El Niño–Southern Oscillation variance over the past six centuries, *Clim.*
769 *Past*, 9(5), 2269–2284, doi:10.5194/cp-9-2269-2013.
- 770 Moy, C. M., G. O. Seltzer, D. T. Rodbell, and D. M. Anderson (2002), Variability of El
771 Niño/Southern Oscillation activity at millennial timescales during the Holocene epoch,
772 *Nature*, 420(6912), 159–162, doi:10.1038/nature01163.
- 773 Newton, A., R. Thunell, and L. Stott (2006), Climate and hydrographic variability in the Indo-
774 Pacific Warm Pool during the last millennium, *Geophys. Res. Lett.*, 33(19), 596–5,
775 doi:10.1029/2006GL027234.
- 776 Nurhati, I. S., K. M. Cobb, C. D. Charles, and R. B. Dunbar (2009), Late 20th century warming
777 and freshening in the central tropical Pacific, *Geophys. Res. Lett.*, 36(21), 345–4,
778 doi:10.1029/2009GL040270.
- 779 Parzen, E. (1962), On estimation of a probability density function and mode, *Ann. Math. Stat.*,
780 33(3), 1065–1076, doi:10.2307/2237880?refreqid=search-
781 gateway:8eadc3919de5dc23d224e04fbdeb76c9.
- 782 Pearson, K. (1920), Notes on the history of correlation, *Biometrika*, 13(1), 25,
783 doi:10.2307/2331722.
- 784 Quinn, T. M., and D. E. Sampson (2002), A multiproxy approach to reconstructing sea surface
785 conditions using coral skeleton geochemistry, *Paleoceanography*, 17(4), 14–1–14–11,
786 doi:10.1029/2000PA000528.
- 787 Quinn, T. M., F. W. Taylor, and T. J. Crowley (2006), Coral-based climate variability in the
788 Western Pacific Warm Pool since 1867, *J. Geophys. Res.*, 111(C11), 345–11,
789 doi:10.1029/2005JC003243.
- 790 Quinn, T. M., T. J. Crowley, and F. W. Taylor (1996), New stable isotope results from a 173-
791 year coral from Espiritu Santo, Vanuatu, *Geophys. Res. Lett.*, 23(23), 3413–3416,
792 doi:10.1029/96GL03169.
- 793 Rayner, N. A., D. E. Parker, E. B. Horton, C. K. Folland, L. V. Alexander, and D. P. Rowell
794 (2003), Global analyses of sea surface temperature, sea ice, and night marine air temperature
795 since the late nineteenth century, *J. Geophys. Res.*, 108(D14), 14–37,
796 doi:10.1029/2002JD002670.
- 797 Rein, B., A. Lückge, and F. Sirocko (2004), A major Holocene ENSO anomaly during the
798 Medieval period, *Geophys. Res. Lett.*, 31(17), doi:10.1029/2004GL020161.

- 799 Reynolds, R. W., and T. M. Smith (1994), Improved global sea surface temperature analyses
800 using optimum interpolation, *J. Clim.*, 7(6), 929–948, doi:10.1175/1520-
801 0442(1994)007<0929:IGSSTA>2.0.CO;2.
- 802 Ropelewski, C. F., and M. S. Halpert (1987), Global and regional scale precipitation patterns
803 associated with the El Niño/Southern Oscillation, *Mon. Weather Rev.*, 115, 1606–1626.
- 804 Rustic, G. T., A. Koutavas, T. M. Marchitto, and B. K. Linsley (2015), Dynamical excitation of
805 the tropical Pacific Ocean and ENSO variability by Little Ice Age cooling, *Science*,
806 350(6267), 1537–1541, doi:10.1126/science.aac9937.
- 807 Santoso, A., M. J. McPhaden, and W. Cai (2017), The defining characteristics of ENSO
808 extremes and the strong 2015/2016 El Niño, *Rev. Geophys.*, 55(4), 1079–1129,
809 doi:10.1002/2017RG000560.
- 810 Schrag, D. P. (1999), Rapid analysis of high-precision Sr/Ca ratios in corals and other marine
811 carbonates, *Paleoceanography*, 14(2), 97–102, doi:10.1029/1998PA900025.
- 812 Shen, C.-C. et al. (2012), High-precision and high-resolution carbonate ²³⁰Th dating by MC-ICP-
813 MS with SEM protocols, *Geochim. Cosmochim. Acta*, 99(C), 71–86,
814 doi:10.1016/j.gca.2012.09.018.
- 815 Taylor, F. W., C. Fröhlich, J. Lecolle, and M. Strecker (1987), Analysis of partially emerged
816 corals and reef terraces in the central Vanuatu arc: Comparison of contemporary coseismic
817 and nonseismic with Quaternary vertical movements, *J. Geophys. Res.*, 92, 4905–4933,
818 doi:10.1029/JB092iB06p04905.
- 819 Taylor, F. W., R. L. Edwards, G. J. Wasserburg, and C. Frohlich (1990), Seismic recurrence
820 intervals and timing of aseismic subduction inferred from emerged corals and reefs of the
821 Central Vanuatu (New Hebrides) Frontal Arc, *J. Geophys. Res.*, 95(B1), 393–408,
822 doi:10.1029/JB095iB01p00393.
- 823 Thirumalai, K., A. Singh, and R. Ramesh (2011), A MATLAB™ code to perform weighted
824 linear regression with (correlated or uncorrelated) errors in bivariate data, *J. Geol. Soc.*
825 *India*, 77(4), 377–380, doi:10.1007/s12594-011-0044-1.
- 826 Thirumalai, K., F. W. Taylor, C.-C. Shen, L. L. Lavier, C. Frohlich, L. M. Wallace, C.-C. Wu, H.
827 Sun, and A. K. Papabatu (2015), Variable Holocene deformation above a shallow subduction
828 zone extremely close to the trench, *Nat. Commun.*, 6(1), 1–6, doi:10.1038/ncomms8607.
- 829 Thirumalai, K., J. N. Richey, T. M. Quinn, and R. Z. Poore (2014), *Globigerinoides ruber*
830 morphotypes in the Gulf of Mexico: A test of null hypothesis, *Sci. Rep.*, 4(1), 423–7,
831 doi:10.1038/srep06018.
- 832 Thirumalai, K., J. W. Partin, C. S. Jackson, and T. M. Quinn (2013), Statistical constraints on El
833 Niño Southern Oscillation reconstructions using individual foraminifera: A sensitivity
834 analysis, *Paleoceanography*, 28(3), 401–412, doi:10.1002/palo.20037.

- 835 Torrence, C., and G. Compo (1998), A practical guide to wavelet analysis, *Bull. Amer. Meteor.*
836 *Soc.*, 79(1), 61–78, doi:10.1175/1520-0477(1998)079<0061:APGTWA>2.0.CO;2.
- 837 Trenberth, K. E. (1976), Spatial and temporal variations of the Southern Oscillation, *Q.J.R.*
838 *Meteorol. Soc.*, 102(433), 639–653, doi:10.1002/qj.49710243310.
- 839 Trenberth, K. E. (1997), The definition of El Niño, *Bull. Amer. Meteor. Soc.*, 78(12), 2771–2777,
840 doi:10.1175/1520-0477(1997)078<2771:TDOENO>2.0.CO;2.
- 841 Trenberth, K. E., and T. J. Hoar (1996), The 1990–1995 El Niño–Southern Oscillation event:
842 Longest on record, *Geophys. Res. Lett.*, 23(1), 57–60, doi:10.1029/95GL03602.
- 843 Trenberth, K. E., J. M. Caron, D. P. Stepaniak, and S. Worley (2002), Evolution of El Niño–
844 Southern Oscillation and global atmospheric surface temperatures, *J. Geophys. Res.*, 107,
845 doi:10.1029/2000JD000298.
- 846 Tudhope, A. W. (2001), Variability in the El Niño–Southern Oscillation through a glacial-
847 interglacial cycle, *Science*, 291(5508), 1511–1517, doi:10.1126/science.1057969.
- 848 Wittenberg, A. T. (2009), Are historical records sufficient to constrain ENSO simulations?
849 *Geophys. Res. Lett.*, 36(12), 3–5, doi:10.1029/2009GL038710.
- 850 Wolter, K., and M. S. Timlin (2011), El Niño/Southern Oscillation behaviour since 1871 as
851 diagnosed in an extended multivariate ENSO index (MEI.ext), edited by S. Gulev, *Int. J.*
852 *Climatol.*, 31(7), 1074–1087, doi:10.1002/joc.2336.

Submitted to Paleoceanography and Paleoclimatology on July 31, 2019

Supporting Information for

A century of reduced ENSO variability during the Medieval Climate Anomaly

A.E. Lawman^{1,2*}, T.M. Quinn^{1,2}, J.W. Partin¹, K. Thirumalai^{1,3}, F.W. Taylor¹, C.-C. Wu^{4,5}, T.-L. Yu^{4,5},
M.K. Gorman^{1,2}, C.-C. Shen^{4,5}

¹Institute for Geophysics, Jackson School of Geosciences, The University of Texas at Austin, Austin, TX, USA, ²Department of Geological Sciences, Jackson School of Geosciences, The University of Texas at Austin, Austin, TX, USA, ³Department of Earth, Environmental and Planetary Sciences, Brown University – Providence, RI, USA, ⁴High-precision Mass Spectrometry and Environment Change Laboratory (HISPEC), National Taiwan University, Taipei, Taiwan ROC, ⁵Research Center for Future Earth, National Taiwan University, Taipei, Taiwan ROC

Contents of this file

Figures S1 to S8
Table S1

Introduction

The supporting information includes metadata about the modern and fossil corals, including x-ray images (Figure S1, Table S1). The supporting information also covers the results of the calibration-verification exercise for converting coral Sr/Ca measurements into sea surface temperature (SST; Figure S2). The agreement between the replicated MCA fossil coral Sr/Ca time series is provided (Figure S3). An example of the output from the Monte Carlo uncertainty quantification algorithm is provided for the Sabine Bank, Vanuatu modern coral Sr/Ca-SST reconstruction (Figure S4). The fidelity of the differences in the 2.5 and 97.5 percentile SSTA populations, or the magnitude of extreme events, is explored for the modern and MCA (Figures S5-S7). An informal test of the 'Wittenberg effect' [Wittenberg, 2009] is performed to show how the values for extreme events may vary according to window length (Figure S8).

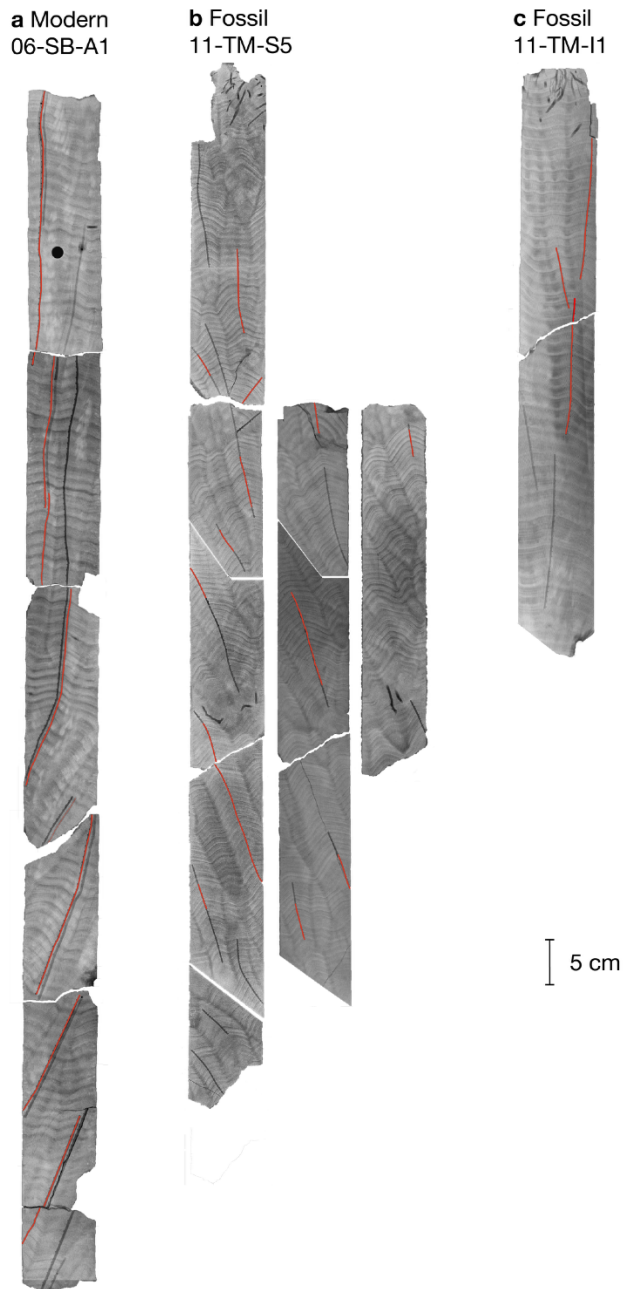


Figure S1. Coral x-radiographs and sampling paths. X-ray images of 5 mm thick slabs from modern coral 06-SB-A1 (**a**), fossil coral 11-TM-S5 (**b**), and fossil coral 11-TM-I1 (**c**). The modern core in **a** was collected from a live *Porites lutea* coral head at Sabine Bank, Vanuatu during a drilling expedition in 2006. The fossil corals in **b**, **c** were collected from the same uplifted reef at Tasmaloum, Vanuatu but from different coral heads during a drilling expedition in 2011. The adjacent slabs to the right of the first slabs in **b** are additional cross-sectional slabs taken from the core to fill in gaps with suboptimal sampling. The solid red lines indicate sampling paths along the coral's maximum growth axis. The non-colored paths indicate suboptimal sampling paths [DeLong *et al.*, 2013]. The final composite includes data only from the red paths. Scale bar represents 5 cm.

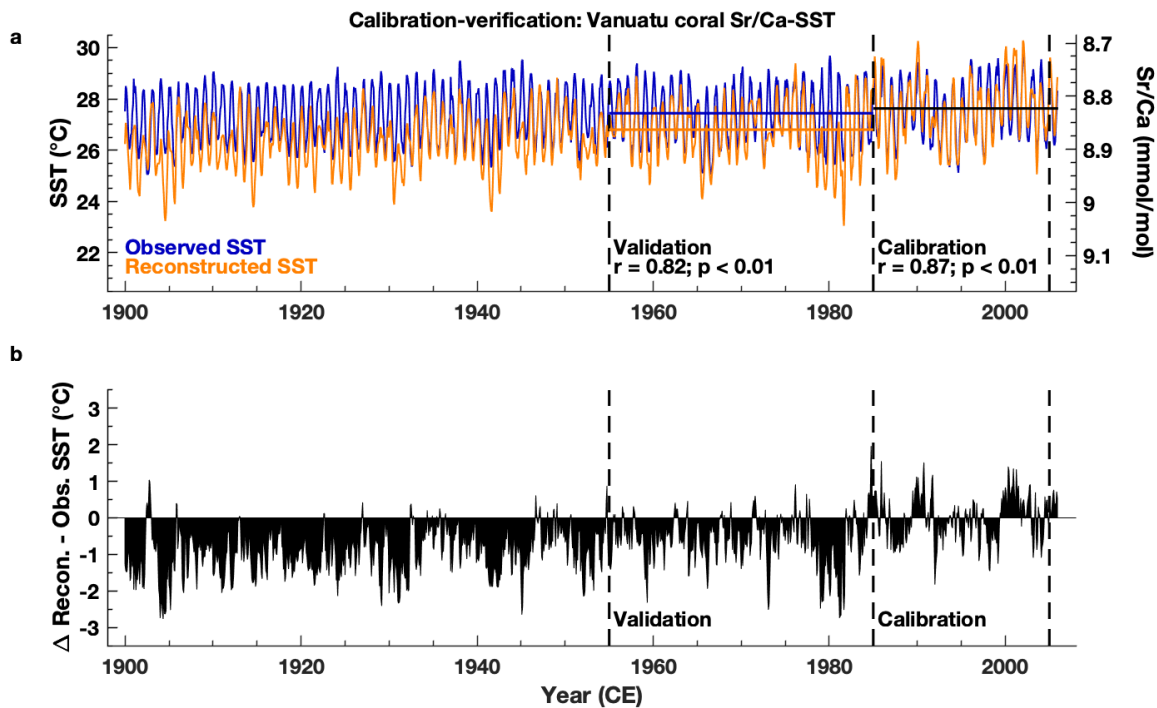


Figure S2. Modern coral SST calibration and verification. **a** Instrumental SST [Rayner *et al.*, 2003] (blue, see Fig. 3) and reconstructed Sabine Bank, Vanuatu (15.9°S, 166.0°E) modern coral Sr/Ca-SST (orange; Fig. 4; Section 3.2). Left axis SST (°C), right axis coral Sr/Ca (mmol/mol). Dashed vertical lines mark the calibration (1985-2005 CE) and verification (1955-1984 CE) intervals (Section 3.2). The black horizontal line indicates the observed/reconstructed median SST value over the calibration window. The colored horizontal lines indicate the median SST values over the verification windows for observed SST (blue) and reconstructed coral Sr/Ca-SST (orange). Calibration equation: $SST (^{\circ}C) = -20.73 \times \text{Coral Sr/Ca (mmol/mol)} + 210.53$. The 1985-2005 CE calibration interval maximizes the correlation [Pearson, 1920] with instrumental SST ($r = 0.87$, $p < 0.01$) and minimizes the residual sum of squares over the 1955-1984 CE verification window (Section 3.2). **b** The difference between the modern Sabine Bank coral SST reconstruction and observed SST. Much of the difference on interannual to decadal timescales stems from the lack of observations (Fig. 3), including the smaller global warming trend in observations, as compared to the coral. The coral trend of $0.83^{\circ}C/50$ years at Sabine Bank resembles the trend of $0.5\text{--}0.75^{\circ}C/50$ years seen in observations for the southwest Pacific [Cravatte *et al.*, 2009].

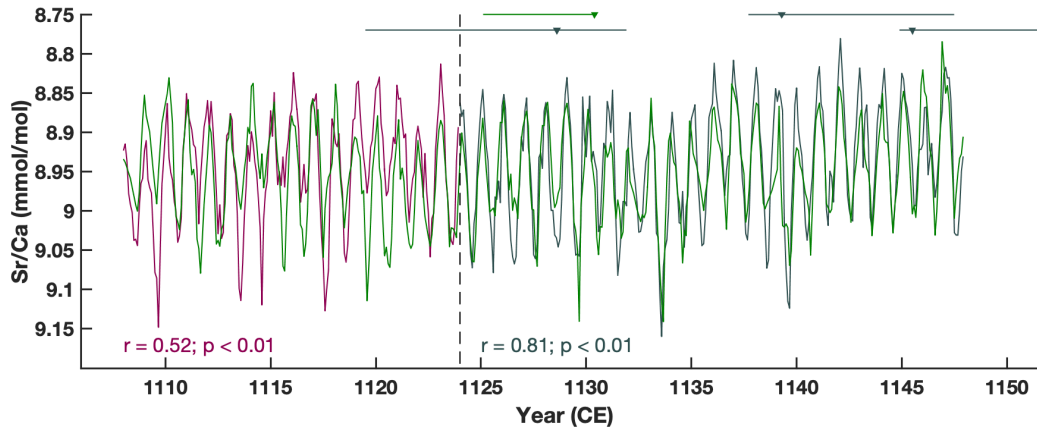


Figure S3. Replicated fossil coral Sr/Ca during part of the Medieval Climate Anomaly. Sr/Ca time series for fossil coral 11-TM-S5 (green; $^{230}\text{Th} \pm 2\sigma$ age: 1127.1 ± 2.7 CE) and the shorter replication coral 11-TM-I1 ($^{230}\text{Th} \pm 2\sigma$ ages: 1125.7 ± 6.2 , 1142.6 ± 4.9 , 1149.0 ± 4.1 CE) over their common interval of overlap (1108-1147 CE). Section of 11-TM-I1 data that passed the quality control metrics outlined by *DeLong et al.* [2013] (gray, 1124-1147 CE) and is included in the final Sr/Ca composite. Section of 11-TM-I1 data that did not pass the quality control metrics (magenta, 1108-1123 CE) due to stress banding and a lack of clearly defined theca walls that help identify the maximum growth axis in the x-ray image (Figure S1). Dashed vertical black line separates the sections with optimal and sub-optimal sampling of 11-TM-I1. To yield a reliable climate reconstruction, sections with sub-optimal sampling are excluded from the final coral records presented in the main text. Triangles with horizontal bars mark the ^{230}Th ages and $\pm 2\sigma$ analytical error. The fossil coral Sr/Ca time series were shifted within the analytical error ($\pm 2\sigma$) of the four ^{230}Th ages such that the resulting overlap between 11-TM-S5 and 11-TM-I1 achieved the highest Pearson correlation coefficient [*Pearson, 1920*] ($r = 0.81$, $p < 0.01$) over the 1124-1147 CE interval that includes coral data that passed all quality control metrics. The Pearson correlation coefficient is lower ($r = 0.52$) for the 1108-1123 CE interval that includes data from 11-TM-I1 that did not pass all quality control metrics.

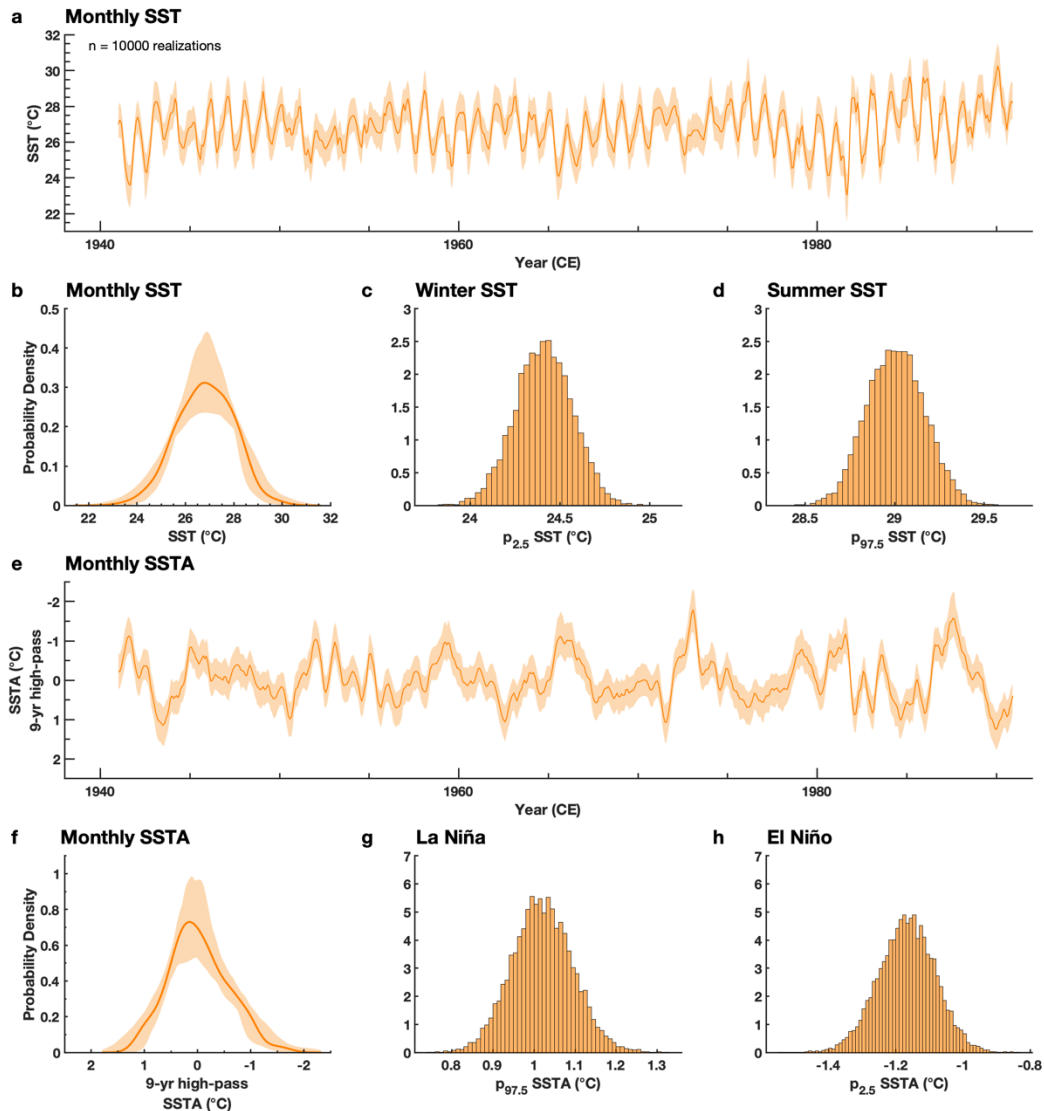


Figure S4. Monte Carlo uncertainty quantification for modern coral Sr/Ca-SST. **a** The modern Sabine Bank Sr/Ca-SST reconstruction for the 1941-1990 CE replication interval with no uncertainty (dark orange) and with realizations (light orange shading) that take analytical and calibration uncertainty into account ($n = 10,000$ realizations; Section 3.4). **b** PDF estimate of the SST reconstruction (dark orange) with realizations (light orange). **c, d** Histograms showing the distribution of possible $p_{2.5}$ (**c**) and $p_{97.5}$ (**d**) SST values based on 10,000 realizations of the SST series. **e** Realizations of the modern Sabine Bank SSTA series (light orange shading) with the SSTA reconstruction with no uncertainty (dark orange). **f** PDF estimates of the SSTA realizations (light orange) and no uncertainty (dark orange). **g, h** Histograms showing the distribution of $p_{97.5}$ (**g**) and $p_{2.5}$ (**h**) SSTA values. Monthly anomalies are computed by applying a 9-year high-pass filter to the SST data, removing the climatology, and computing the 5-month running mean SSTA (Section 3.3). The uncertainty in the SSTA percentiles due to analytical and calibration uncertainty is the average $\pm 2\sigma$ value (± 0.15 °C) from **g, h**.

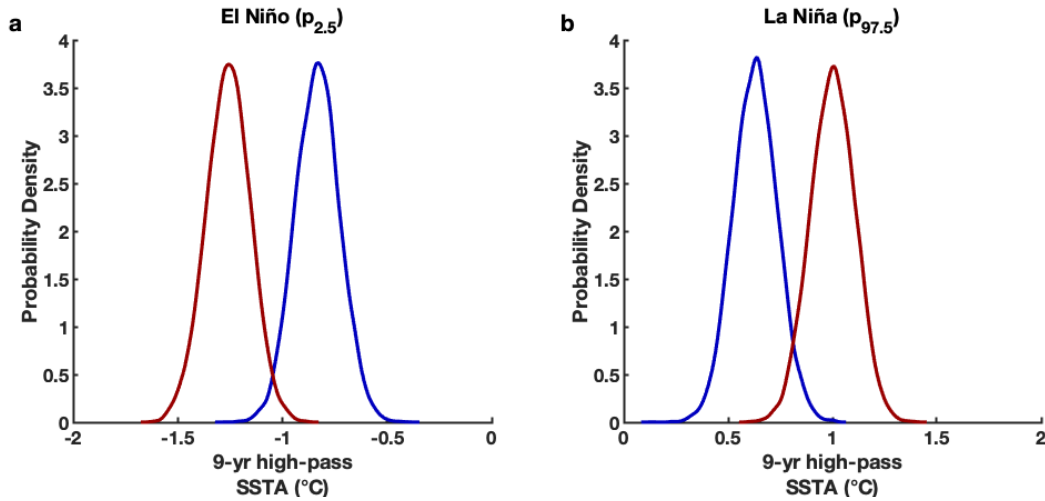


Figure S5. Comparison of Modern (less ENSO variability) and Modern (more ENSO variability) extrema. Gaussian distributions ($n = 10,000$) of the 2.5 (**a**) and 97.5 (**b**) percentiles for modern SW Pacific coral Sr/Ca-SSTA with their computed uncertainties. PDFs show the overlap between the percentiles in Fig. 7, taking uncertainty into account. **a** El Niño-related SSTA ($p_{2.5}$). **b** La Niña-related SSTA ($p_{97.5}$). PDF for the 20th century interval with more (red: 1980-1999 CE) and less (blue: 1920-1939 CE) ENSO variability (**a, b**). The mean percentile values for each PDF in **a, b** are from Fig. 7. The $\pm 2\sigma$ uncertainty in the 2.5 and 97.5 percentiles (width of the PDFs) is ± 0.21 °C based on analytical, calibration, and replication uncertainty (Section 3.4). The overlap between the modern (less variable) and modern (more variable) distributions show that the differences in ENSO variability are large outside of the calculated uncertainty.

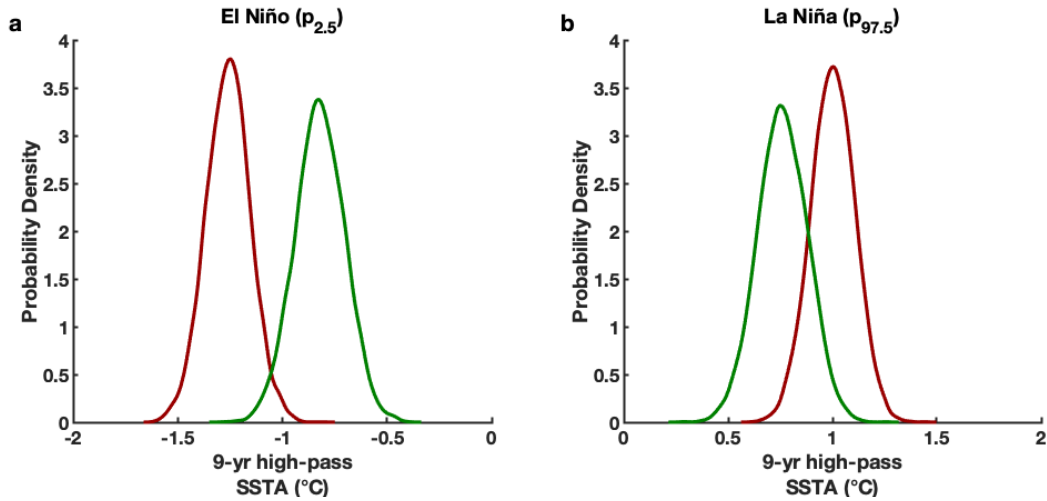


Figure S6. Comparison of Modern (more ENSO variability) and MCA (100 years) extrema. Gaussian distributions ($n = 10,000$) of the 2.5 (**a**) and 97.5 (**b**) percentiles for the modern interval with more ENSO variability (red: 1980-1999 CE) and the MCA (green: 100 years) based on coral Sr/Ca-SSTA. The mean percentile values for each PDF in **a**, **b** are from Fig. 7. The $\pm 2\sigma$ uncertainty in the 2.5 and 97.5 percentiles (width of the PDFs) is ± 0.21 °C (modern) and ± 0.24 °C (MCA) based on analytical, calibration, and replication uncertainty (Section 3.4). **a** El Niño-related SSTA ($p_{2.5}$). **b** La Niña-related SSTA ($p_{97.5}$). The overlap between the PDFs for the modern (more variable) and MCA is smaller compared to the overlap between the modern (less variable) and the MCA (Supplementary Fig. 5), particularly for El Niño related SSTA (**a**). Incorporating the total uncertainty, ENSO variability during the MCA is different than the interval with more ENSO variability during the late 20th century.

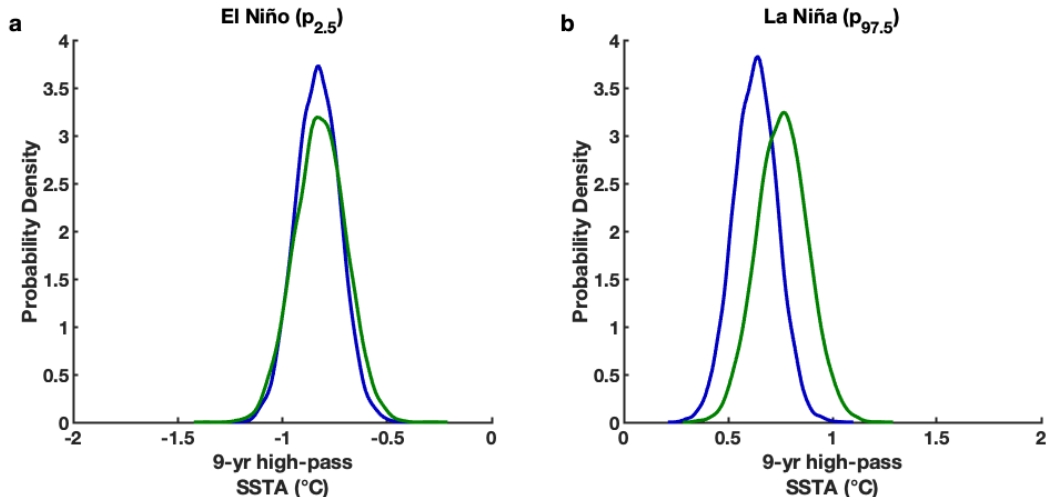


Figure S7. Modern (less ENSO variability) and MCA (100 years) extrema. Gaussian distributions ($n = 10,000$) of the 2.5 (**a**) and 97.5 (**b**) percentiles for the modern interval with less ENSO variability (blue: 1920-1939 CE) and the MCA (green: 100 years) based on coral Sr/Ca-SSTA. The mean percentile values for each PDF in **a**, **b** are from Fig. 7. The $\pm 2\sigma$ uncertainty in the 2.5 and 97.5 percentiles (width of the PDFs) is ± 0.21 °C (modern) and ± 0.24 °C (MCA) based on analytical, calibration, and replication uncertainty (Section 3.4). **a** El Niño-related SSTA ($p_{2.5}$). **b** La Niña-related SSTA ($p_{97.5}$). Incorporating the total uncertainty in the percentiles, ENSO variability during the MCA is similar to the interval with less ENSO variability during the early 20th century.

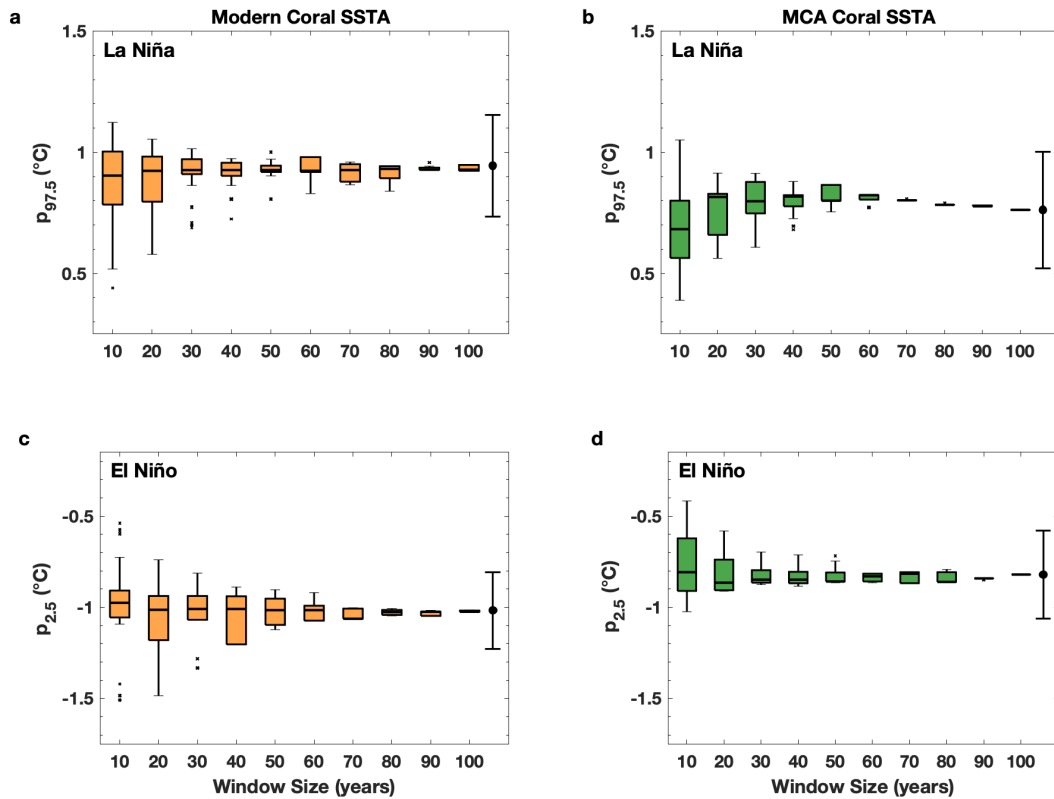


Figure S8. Effect of interval length on variability metrics. **a-d** Box plots summarizing the 97.5 (**a, b**) and 2.5 (**c, d**) percentile values of reconstructed SSTA computed in sliding windows (x-axis) for the Sabine Bank modern coral (**a, c**), and the Tasmaloum fossil coral 11-TM-S5 (**b, d**). All sliding windows are shifted by 1 year. The lower and upper bounds of the boxes correspond to the 25th and 75th percentiles and the center line indicates the median. The whiskers represent the 1.5 x inter-quartile range (IQR). Values greater than 1.5 x IQR are plotted as outliers (black dots). The median $p_{2.5}$ and $p_{97.5}$ values (horizontal black bar) stays relatively constant as a function of window side, justifying our choice to compare 100 years of MCA data to 20 years of modern data (Fig. 7). The black error bars to the right of the 100-year window in a-d indicate the ± 0.21 °C (modern) and ± 0.24 °C (MCA) total uncertainty in the SSTA $p_{2.5}$ and $p_{97.5}$ values taking analytical, calibration, and replication uncertainty into account (Section 3.4). The larger the interdecadal changes in ENSO variability due to natural causes, i.e. the ‘Wittenberg effect, [Wittenberg, 2009]’ the larger the size of the box at smaller window sizes.

core name	coral type/species	site name	location	selected coral pieces	total length (cm)	U-Th date $\pm 2\sigma$ (CE)	U-Th date midpoint (cm)	growth rate (avg. $\pm 2\sigma$, cm/yr)	target temporal resolution	sampling resolution (mm)
06-SB-A1	modern (<i>P. lutea</i>)	SBV ^a	15.9 °S, 166.0 °E	a, b, c, d, e(1)	132.5	--	--	1.19 \pm 0.19	~monthly	1.0
11-TM-S5 ^b	fossil (<i>P. lutea</i>)	TMV ^c	15.6 °S, 166.9 °E	a, b, c	114.4	1127.1 \pm 2.7	36.4	0.73 \pm 0.09	~monthly	0.5, 0.6 ^d
11-TM-I1 ^b	fossil (<i>P. lutea</i>)	TMV ^c	15.6 °S, 166.9 °E	a	62.2	1125.7 \pm 6.2 1142.6 \pm 4.9 1149.0 \pm 4.1	30.5 18.0 10.7	1.24 \pm 0.09	~monthly	0.9

^a SBV: Sabine Bank, Vanuatu

^b Fossil coral cores 11-TM-S5 and 11-TM-I1 were collected from the same uplifted reef but different coral heads

^c TMV: Tasmaloum, Vanuatu

^d The 11-TM-S5 sampling resolution was adjusted for each piece depending on the average growth rate

Table S1. Coral selection, U-Th dating, and sampling information.

References

Cravatte, S., T. Delcroix, D. Zhang, M. McPhaden, and J. Leloup (2009), Observed freshening and warming of the western Pacific Warm Pool, *Clim Dyn*, 33(4), 565–589, doi:10.1007/s00382-009-0526-7.

DeLong, K. L., T. M. Quinn, F. W. Taylor, C.-C. Shen, and K. Lin (2013), Improving coral-base paleoclimate reconstructions by replicating 350 years of coral Sr/Ca variations, *Palaeogeogr. Palaeoclimatol. Palaeoecol.*, 373(C), 6–24, doi:10.1016/j.palaeo.2012.08.019.

Pearson, K. (1920), Notes on the history of correlation, *Biometrika*, 13(1), 25, doi:10.2307/2331722.

Rayner, N. A., D. E. Parker, E. B. Horton, C. K. Folland, L. V. Alexander, and D. P. Rowell (2003), Global analyses of sea surface temperature, sea ice, and night marine air temperature since the late nineteenth century, *J. Geophys. Res.*, 108(D14), 14–37, doi:10.1029/2002JD002670.

Wittenberg, A. T. (2009), Are historical records sufficient to constrain ENSO simulations? *Geophys. Res. Lett.*, 36(12), 3–5, doi:10.1029/2009GL038710.